ABSTRACT

SUBLIMATION PRESSURES OF
SOLID ARGON, KRYPTON, AND XENON.

By

Charles William Leming

An experiment was performed to measure the sublimation pressures of solid argon, krypton, and xenon over wide temperature and pressure ranges. Data are reported from near the respective triple points to about (2.3×10^{-6} Torr, 25.506K) for Ar; (2.1×10^{-4}Torr, 43.130K) for Kr; (3.8×10^{-4}Torr, 70.705K) for Xe. Pressures were measured with a mercury manometer, a McLeod gauge, and a calibrated Bourdon gauge. The pressure measurements were corrected for thermomolecular flow and streaming. Temperatures were measured with a National Bureau of Standards calibrated platinum resistance thermometer using the 1968 International Practical Temperature Scale. The required sample temperatures were achieved by means of a liquid oxygen bath above 55K and by means of a liquid helium bath below 55K. Electrical heating from an ac bridge temperature controller was used to regulate the sample chamber temperature.

Samples were condensed from Matheson research grade gases. Impurity concentrations were reduced by distilling the samples in situ. The gas handling system and sample chamber were constructed so that contamination of the sample by adsorbed gases could be minimized.

Application of the law of corresponding states was investigated by analyzing the reduced pressure curves. Values for static lattice energy, geometric mean of the lattice vibrational spectrum, heat of sublimation, and lattice vibrational energy are calculated using theoretical sublimation pressure curves. Corrections were applied to these values to account for the effect of vacancies.

SUBLIMATION PRESSURES OF SOLID ARGON, KRYPTON, AND XENON.

By

Charles William Leming

A THESIS

Submitted to

Michigan State University

in partial fulfillment of the requirements

for the degree of

DOCTOR OF PHILOSOPHY

Department of Physics

1970

To Paula

ACKNOWLEDGEMENTS

This experiment was suggested by Professor G. L. Pollack. I am very much indebted to him for his guidance and encouragement. Thanks are also due to Mr. Carl James Duthler and Mr. Garold Fritz for assistance in taking data. Also I wish to thank my wife, Paula, for assistance with foreign language materials and help with typing of the thesis. Finally I would like to acknowledge the financial support of the U.S. Atomic Energy Commission.

TABLE OF CONTENTS

LIST OF TABLES

(List of Tables continued)

LIST OF FIGURES

(List of Figures continued)

I. INTRODUCTION

Properties of the rare-gas solids have long created much interest because the nature of the attractive forces between atoms is simple and rather well understood.[1,2] These forces may be approximated as short range, pairwise additive, central forces which have the same form for all the rare gases.[3] Many thermodynamic properties of these solids have been predicted on the basis of simple models. Deviations in the experimental data may be used to study such details as anharmonicity,[4,5] electron exchange,[6] and lattice defects.[7,8]

Although lending themselves well to simple theoretical models, experimental studies of the rare-gas solids have met with many difficulties. Because the triple point temperatures of rare gases are relatively low, low temperature techniques must be applied to study these solids.

The purpose of this experiment was to provide accurate sublimation pressure data extending over several orders of magnitude for each of the rare-gas solids. In order to accomplish this, a low temperature cryostat was constructed to operate in the temperature range from 200K to 20K. Measurements for all gases were made using this apparatus.

These data have been analyzed on the basis of vapor

pressure curves predicted by classical thermodynamics[9] and vapor pressure curves predicted by lattice dynamical theory.[7] From this analysis values were calculated for heats of fusion, vibrational energies, static lattice energies, and for the geometric mean of the lattice vibrational spectra. The law of corresponding states has been applied to test the consistency of published potential parameters for Ar, Kr, and Xe.

This thesis describes the experiment and calculations. Results of this experiment are reported in terms of parameters for vapor pressure curves and also tables of primary data.

II. THEORETICAL

General Properties of Rare-Gas Solids

Many calculations have been performed to predict the thermodynamic properties of rare-gas solids. The reason for this theoretical interest is that the forces between the atoms may be closely approximated as simple central forces which have the same form for all the rare gases.[3] Forces of this type are a good first approximation because the atoms consist of tightly bound, filled electronic orbitals.

For dilute gases, central forces can be applied almost exactly. For solids, however, the possibility exists that the actual intermolecular forces may consist of various nonadditive three-body forces in addition to the expected two-body forces.

The interatomic potentials which are normally used to calculate properties of the solids are central potentials which have adjustable parameters. These parameters are used to fit theoretical calculations to experimentally determined thermodynamic properties of the solid. Thus, the parameters are chosen as if the actual potential were a central potential. However, it must be remembered that these parameters are only effective parameters which result from assuming no three-body effects are present. The

actual potential may contain three-body effects so that the assumed two-body potential cannot perfectly represent the actual potential. Therefore, the two-body potential can only be adjusted to give as good a fit as possible.

Because the actual potential cannot be calculated, many analytical potentials have been suggested to represent the intermolecular forces. The simplest and most commonly used form is the well known Mie—Lennard-Jones potential given by[3]:

$$\mathcal{U}(r) = \frac{mn\epsilon}{m-n}\left\{\frac{1}{m}\left(\frac{r_o}{r}\right)^m - \frac{1}{n}\left(\frac{r_o}{r}\right)^n\right\} \quad . \quad (1)$$

Here, $-\epsilon$ is the depth of the potential and r_o is the distance from the origin to the lowest point in the potential well. The values of m and n are usually taken to be 12 and 6 respectively.

The n=6 attractive potential at large separations can be calculated from the induced dipole - induced dipole interaction as calculated by London using second-order perturbation theory.[10] For this calculation, ground state wave functions are assumed and higher order attractions are neglected.

Although the attractive part of the Mie—Lennard-Jones potential is theoretically plausible, the repulsive part has no such satisfactory theoretical basis. An accurate calculation of the repulsion due to overlapping electron wave functions would most likely yield an exponential form for the repulsion.[3] However, in order to simplify computations, the value m=12 is usually chosen for the exponent of

the repulsive term. In this case the Mie—Lennard-Jones potential becomes: $\varphi(r) = \epsilon\left\{\left(\frac{r_o}{r}\right)^{12} - 2\left(\frac{r_o}{r}\right)^{6}\right\}$. (2)

Other forms of the binding potential include the Buckingham potential given by [11]

$$\varphi(r) = \frac{6m\epsilon}{m-6}\left\{\frac{1}{m}\exp\left[-m\,(r/r_o)-1\right] - \frac{1}{6}\left(\frac{r_o}{r}\right)^{6}\right\}. \quad (3)$$

Here, m, r_o, and ϵ have the same meaning as in the Mie—Lennard-Jones potential. Although this potential seems more acceptable physically, it is not often used because of computational difficulties. Also this potential does not seem to give significantly superior theoretical predictions.

Other potentials such as the Morse potential[12] and the Munn-Smith[13] potential have been considered as likely potentials to represent rare-gas solids. Neither the Morse potential nor the Munn-Smith potential deviate greatly from the potentials described previously.

The parameters ϵ and r_o are usually determined from experimental values of the sublimation energy and lattice parameter at 0 K.[14] Typical values of ϵ and r_o for the Mie—Lennard-Jones potential and the Buckingham potential are found in Table 1 and Table 2 respectively. The results are presented both for the case when the potentials act between all neighbors and also for the case when the potentials act between nearest neighbors only.[3] Since the potentials considered are only estimates of what may actually be happening in the crystal, neither

model is obviously superior.[15]

TABLE 1

Values[a] of the Mie—Lennard-Jones potential parameters ϵ and r_o for m = 12, n = 6.

	Argon	Krypton	Xenon
	(All Neighbor)		
ϵ (10^{-16}erg)	165	227	319
r_o (10^{-8}cm)	3.820	4.084	4.446
	(Nearest Neighbor)		
ϵ (10^{-16}erg)	236	325	458
r_o (10^{-8}cm)	3.709	3.966	4.318

[a]Ref. 3.

TABLE 2

Values[a] of the Buckingham potential parameters ϵ and r_o for m = 12.

	Argon	Krypton	Xenon
	(All Neighbor)		
ϵ (10^{-16}erg)	160.9	222.8	314.3
r_o (10^{-8}cm)	3.855	4.121	4.485
	(Nearest Neighbor)		
ϵ (10^{-16}erg)	222.2	323.6	456.6
r_o (10^{-8}cm)	3.712	3.968	4.319

[a]Ref. 3.

Although the equation of state of solids cannot yet be calculated from any known analytic potential, certain aspects of the equation of state can be investigated by applying the law of corresponding states. This law shows that the equations of state for simple substances are identical when expressed in terms of suitable non-dimensional reduced variables.

If classical statistical mechanics applies, the equation of state for simple molecules becomes a function of reduced temperature, Tr, reduced pressure, Pr, and reduced volume, Vr.[16] Thus the equation of state may be written

$$Pr = Pr\,(Vr, Tr) \quad \cdot \quad (4)$$

The reduced variables are found by dividing P, V, and T respectively by the corresponding critical constants P_c, V_c, and T_c so that:

$$Pr = {}^{P}/_{P_c}, \quad Vr = {}^{V}/_{V_c}, \quad \text{and} \quad Tr = {}^{T}/_{T_c} \quad \cdot \quad (5)$$

This form of the law of corresponding states has been found to apply mainly to simple gases and liquids. Solids generally deviate from this law.

A more modern form of the law of corresponding states has been found to be applicable to some solids. Consider spherically symmetric molecules whose potential energies depend only on the intermolecular separation and have the form $\mathcal{Q}(r) = \epsilon\, f({}^{r}/_{\sigma})$. For such substances the equations of state may be expressed in terms of the modern reduced variables:

$$P^* = P\sigma^3/\epsilon\,, \quad V^* = V/N\sigma^3, \quad T^* = {}^{kT}/_{\epsilon} \quad \cdot \quad (6)$$

Here ϵ is the depth of the intermolecular potential well and σ is a characteristic length for which $\mathcal{Q}(r=\sigma) = 0$.

This form of the law of corresponding states is derived from quantum statistical mechanics.[17,18] The partition function $\mathcal{Z}$ can be calculated from the sum

over states

$$Z = \sum_{\eta} \exp(-E_n/kT) \quad \cdot \quad (7)$$

Here E_n are the steady state energy levels determined from the eigenvalues of the Schrödinger equation of the system. The Schrödinger equation for a system of N interacting spherically symmetric molecules is

$$\left[-(\hbar^2/2m)\sum_{i=1}^{N}\nabla_i^2 + \sum_{i>k} \mathcal{Q}(r_{ik}) - E_n\right]\psi_\eta(r_1 \cdots r_N) = 0 \cdot \quad (8)$$

Written in terms of non-dimensional reduced variables $E_n^* = E_n/N\epsilon$, $f(r^*) = \mathcal{Q}/\epsilon$, and $\nabla_i^{*2} = \sigma^2\nabla_i^2$, the equation becomes

$$\left[-\Lambda^{*2}\sum_{i=1}^{N}\left(\frac{1}{8\pi^2}\right)\nabla_i^{*2} + \sum_{i>k} f(r_{ik}^*) - NE_n^*\right]\psi_n(r_1^*, \cdots, r_N^*) = 0 \quad \cdot \quad (9)$$

In equation (9) Λ^* is the reduced de Broglie wavelength given by

$$\Lambda^* = h/\sigma(m\epsilon)^{\frac{1}{2}} \quad \cdot \quad (10)$$

As can be seen from the form of equation (9), the reduced eigenvalues E_n^* depend on V^* and Λ^*.

The partition function can then be written in terms of reduced variables.

$$Z = \sum_{\eta} \exp\left[-E_n^*/(kT/\epsilon)\right] = \sum_{\eta} \exp -E_n^*/T^* \quad \cdot \quad (11)$$

From this it follows that

$$Z = Q(V^*, T^*, \Lambda^*) \quad \cdot \quad (12)$$

The equation of state can be calculated from the partition function using the thermodynamic relationship

$$P^* = \frac{T^*}{N}\frac{\partial \ln Q(V^*, T^*, \Lambda^*)}{\partial V^*} \quad \cdot \quad (13)$$

Thus the equation of state is only a function of reduced

variables and may be written

$$P^* = P^* (V^*, T^*, \Lambda^*) \quad . \quad (14)$$

The form of equation (14) is the same for each type of molecule and depends only on the reduced variables P^*, V^*, T^*, and Λ^*.

The values of the parameters ϵ and σ used to calculate the reduced variables depend on the exact form of the potential assumed. Table 3 shows accepted values[3] of ϵ, σ, and Λ^* for the Mie—Lennard-Jones all-neighbor potential. For this potential σ is related to r_o defined earlier by $r_o = 2^{1/6}\sigma$.

TABLE 3

Values[a] of the parameters ϵ, σ, and Λ^* for the Mie—Lennard-Jones all-neighbor potential with m=12, n=6.

	Argon	Krypton	Xenon
ϵ (10^{-16}erg)	165	227	319
σ (10^{-8}cm)	3.503	3.745	4.077
Λ^*	0.0289	0.0158	0.00980

[a]Calculated from parameters presented in reference 3.

The crystal structure of solid rare gases is a property which cannot be predicted using the two-body potentials presented earlier. Both the Mie—Lennard-Jones[19] and Buckingham[20] potentials predict that at T = 0 K rare gases crystallize in the hcp phase. However, experiments at temperatures as low as 2.5K[21] have revealed that the rare-gas crystals have fcc structure with some hcp present as stacking faults.

Several explanations have been given to this crystal structure. Probably the observed fcc structure indicates inaccuracies in the analytic potentials assumed[22] or that three-body effects are significant in these solids.[23]

Vapor Pressure

The condition for vapor-solid equilibrium given by classical thermodynamics is that the specific Gibbs functions, g, of the respective phases must be equal.[24] From this condition it is possible to calculate equations for the vapor pressure of crystals.

Surfaces between solid and vapor phases may also be considered using this principle. It might be asked what effect the exact nature of the processes occuring at the surface between solid and vapor phases has on vapor-solid equilibrium. The solution to this problem is to consider the surface as a separate phase which is different from the solid or vapor. The condition for phase equilibrium may then be extended to become.

$$g(\text{solid}) = g(\text{surface}) = g(\text{vapor})$$

From the above equation it can be seen that the effects of surface properties can be ignored when considering vapor-solid equilibrium. To calculate the conditions for vapor-solid equilibrium, it is only necessary to equate the specific Gibbs functions of the bulk solid and the vapor.

For a monatomic solid, the vapor pressure may be accurately calculated from the Clausius-Clapeyron

equation of classical thermodynamics.[25] This equation may be derived from the condition for vapor- solid equilibrium.

The specific Gibbs function is defined as $g = u - Ts + Pv$. In this equation u is the internal energy and s is specific entropy. The condition for equilibrium then becomes

$$g_c = g_v \quad . \qquad (15)$$

Here the subscript c refers to the solid phase and the subscript v refers to the vapor phase.

If the equilibrium temperature is changed slightly from T to T + dT, the vapor pressure changes from P to P + dP. The condition for maintaining the Gibbs functions equal is then $dg_c = dg_v$. In terms of T and P this may be written

$$-s_c\, dT + v_c\, dP = -s_v\, dT + v_v\, dP \quad . \qquad (16)$$

Taking the ratio dP/dT in equation (16) gives

$$dP/dT = s_c - s_v/v_c - v_v \quad . \qquad (17)$$

Using the definition of specific enthalpy $h = u + Pv$, equation (17) becomes:

$$\frac{dP}{dT} = \frac{(h_c-h_v) - (g_c-g_v)}{T\,(v_c - v_v)} \quad . \qquad (18)$$

However, using the condition for equilibrium, $g_c = g_v$, and the differential relation $d \ln P = dP/P$, equation (18) becomes

$$\frac{d \ln P}{dT} = \frac{h_c - h_v}{T\,(Pv_v)\,(v_c/v_v-1)} \quad . \qquad (19)$$

Using the virial expansion for Pv_v gives:

$$\frac{d \ln P}{dT} = \frac{h_c - h_v}{RT^2 (1 + BP/RT) (v/v_v - 1)} , \quad (20)$$

where B is the second virial coefficient defined by

$$Pv = RT (1 + B/v + \ldots) . \quad (21)$$

Noting that $v_c/v_v \ll 1$ and $BP/RT \ll 1$, equation (20) may be written

$$\frac{d \ln P}{d\, 1/T} = \frac{h_c - h_v}{R (1 - v_c/v_v + BP/RT)} . \quad (22)$$

The difference in enthalpies of the two phases, $h_c - h_v$, is equal to the heat of sublimation, L.

Using equation (22) it is possible to calculate the heat of sublimation of simple molecular solids. Sublimation pressure data may be plotted in the form ln P versus $1/T$. The slope of this plot may then be measured and the heat of sublimation calculated.

Because the slope of this curve varies slowly with temperature, the data can be assumed to be a straight line over narrow temperature ranges. The method of least squares may be used to fit the data to the equation

$$\ln P = a/T + b . \quad (23)$$

The parameter a is then equal to the right side of equation (22).

A slightly different sublimation pressure curve for simple molecular solids may be found from lattice dynamical theory.[7] The partition function for a single harmonic oscillator may be written as a sum over states,

$$z = \sum_{n} \exp(-E_n/kT) \text{ in which } E_n = \hbar\omega\,(n+\tfrac{1}{2}) \quad . \quad (24)$$

Performing the sum over states yields

$$z = \frac{\exp(-\hbar\omega/kT)}{1 - \exp(\hbar\omega/2kT)} \quad . \quad (25)$$

For a system of 3N oscillators, the Helmholtz free energy, F = U-TS, is then

$$F = -\sum_{i=1}^{3N} kT \ln z = \sum_{i=1}^{3N} \frac{\hbar\omega_i}{2} + kT \ln\left[1 - \exp(-\hbar\omega_i/kT)\right] \cdot \quad (25)$$

For an ideal single crystal whose lattice vibrations are assumed to be harmonic, equation (25) gives the thermal contribution of the Helmholtz free energy. To find the total free energy, the static lattice energy, E_o, must be added to this expression. Physically, E_o represents the depth of the potential well binding the solid.

If this equation is then expanded for high temperatures, F can be analytically expressed as

$$F = E_o + 3NkT\left[\ln\frac{\hbar\omega_g}{kT} + \sum_{i=1}^{\infty}(-1)^{n-1}\frac{B_{2n}}{2n(2n)!}\eta_{2n}\left(\frac{\hbar}{kT}\right)^{2n}\right] \quad (27)$$

In this expression η_{2n} are the even positive moments of the frequency spectrum, $\eta_{2n} = \overline{\omega^{2n}}$, B_{2n} are the Bernoulli numbers, and ω_g is the geometric mean of the lattice vibrational spectrum:

$$\omega_g = \left(\prod_{i=1}^{3N}\omega_i\right)^{1/3N} \quad . \quad (28)$$

In statistical mechanics the Gibbs function for a system of N particles is expressed as $G = \mu N$ where μ is the chemical potential. Thus the statistical mechanical equivalent of equation (15) for equilibrium of phases is $\mu_c = \mu_v$. The chemical potential of the

vapor is μ_v.

The chemical potential of the solid, μ_c, is formed from $\mu_c = F/N + Pv_c$. Here, F is the Helmholtz free energy of the crystal. If μ_c is now set equal to the chemical potential of the gas phase, the following expression is found for the equilibrium vapor pressure of an ideal solid.[7]

$$\ln P = -\tfrac{1}{2} \ln T + E_o/NkT + Pv_c/kT + 3 \ln \omega_g + 3 \sum_{n=1}^{\infty} (-1)^{n-1} \frac{B_{2n}}{2n(2n)!} \eta_{2n} \left(\frac{\hbar}{kT}\right)^{2n} \doteq \frac{B}{v_v} + \ln \left[\left(\frac{m}{2\pi}\right)^{3/2} \frac{1}{k^{3/2}} \right]. \quad (29)$$

In this equation m is the atomic mass and B is the second virial coefficient defined in equation (21).

The validity of this equation depends on perfect crystal structure, quasi-harmonic lattice vibrations, and gas imperfection so small that terms higher than the second in the virial expansion may be ignored.

For temperatures higher than one-half the Debye temperature, the expansion in 1/T may be ignored. Respective values of one-half the Debye temperatures, are approximately 42K for Ar, 32K for Kr, and 28K for Xe.[2] Neglecting the crystalline atomic volume in comparison with the vapor phase atomic volume and ignoring gas imperfection, equation (29) can be reduced to the form[7]:

$$\ln PT^{\frac{1}{2}} = a/T + b, \quad (30)$$

where, $a = E_o/Nk$, $b = 3 \ln \omega_g + \tfrac{1}{2} \ln \left[(m/2\pi)^3 \, 1/k\right]$.

Thus the slope of the curve, $\ln PT^{\frac{1}{2}}$ versus $1/T$ yields E_o, the static lattice energy, and the intercept of the curve at $\frac{1}{T} = 0$ yields ω_g, the geometric mean of the lattice vibrational spectrum. The parameters E_o and ω_g depend on volume and thus change slowly with temperature. By using the method of least squares to fit experimental vapor pressure data to equation (30), E_o and ω_g may be calculated.

In calculating the chemical potential which led to equation (30), a perfect crystal structure was assumed. For relatively low temperatures this assumption is valid; however, for temperatures near the triple point the effect of vacancy formation becomes significant. Equation (30) may be corrected for vacancies by considering the change in chemical potential due to vacancy formation.

The change in entropy of a lattice of N molecules due to the introduction of n vacancies is

$$S = k \ln \left[(N+n)! \,/\, N!\, n!\right] \quad . \qquad (31)$$

Thus the Gibbs function for a crystal containing n vacancies may be written[7]

$$G_{vac} = G_c + ng_s - kT \ln \left[(N+n)! \,/\, N!\, n!\right] \quad . \qquad (32)$$

In equation (32) G_{vac} is the Gibbs function for the lattice containing n vacancies, G_c is the Gibbs function for a perfect crystal, and g_s is the Gibbs function for vacancy formation.

The chemical potential of the imperfect lattice is then

$$\mu_{vac} = \partial G_{vac} / \partial N = \mu_c - kT \ln(1+n/N) \quad . \quad (33)$$

If the vacancy concentration, n/N, is small, $n/N \ll 1$, equation (33) becomes

$$\mu_{vac} = \mu_c - kT\, n/N \quad . \quad (34)$$

The equilibrium vacancy concentration is given by $n/N = \exp(-g_s/kT)$. Thus the chemical potential for a simple lattice containing vacancies is

$$\mu_{vac} = \mu_c + kT \exp(-g_s/kT) \quad . \quad (35)$$

If this chemical potential is now used to obtain the vapor pressure equation analogous to equation (30), one gets[7]

$$\ln PT^{\frac{1}{2}} + \exp(-g_s/kT) = a/T + b \quad . \quad (36)$$

The parameters a and b have the same definition as in equation (30). Equation (36) may be used to fit vapor pressure data for temperatures near the triple point where vacancy concentration becomes significant.

III. EXPERIMENTAL

Cryostat Design

In order to perform this experiment over the wide pressure and temperature ranges of interest, it was first necessary to construct a constant temperature cryostat for use in the temperature range 25 - 170K. The most stringent requirement for the cryostat used to measure vapor pressure was the capability of holding the sample temperature stable for long periods of time. This was necessary in order to assure that the sample was in equilibrium with its vapor and that the temperature was uniform throughout the sample. The cryostat also was versatile enough to allow the temperature to be changed easily and uniformly in order to facilitate crystal growth in the sample chamber.

Figure 1 shows a sectional view of the basic construction of our cryostat drawn to scale. The drawing does not show the glass dewars which contain the liquid oxygen bath and the liquid nitrogen outer jacket.

The sample chamber within the massive copper block was connected to the gas-handling system and pressure measuring devices (not shown) by a ¼ in. i.d. stainless steel inlet tube with 0.010 in. wall thickness. This tube was heated by means of a 1000Ω manganin wire

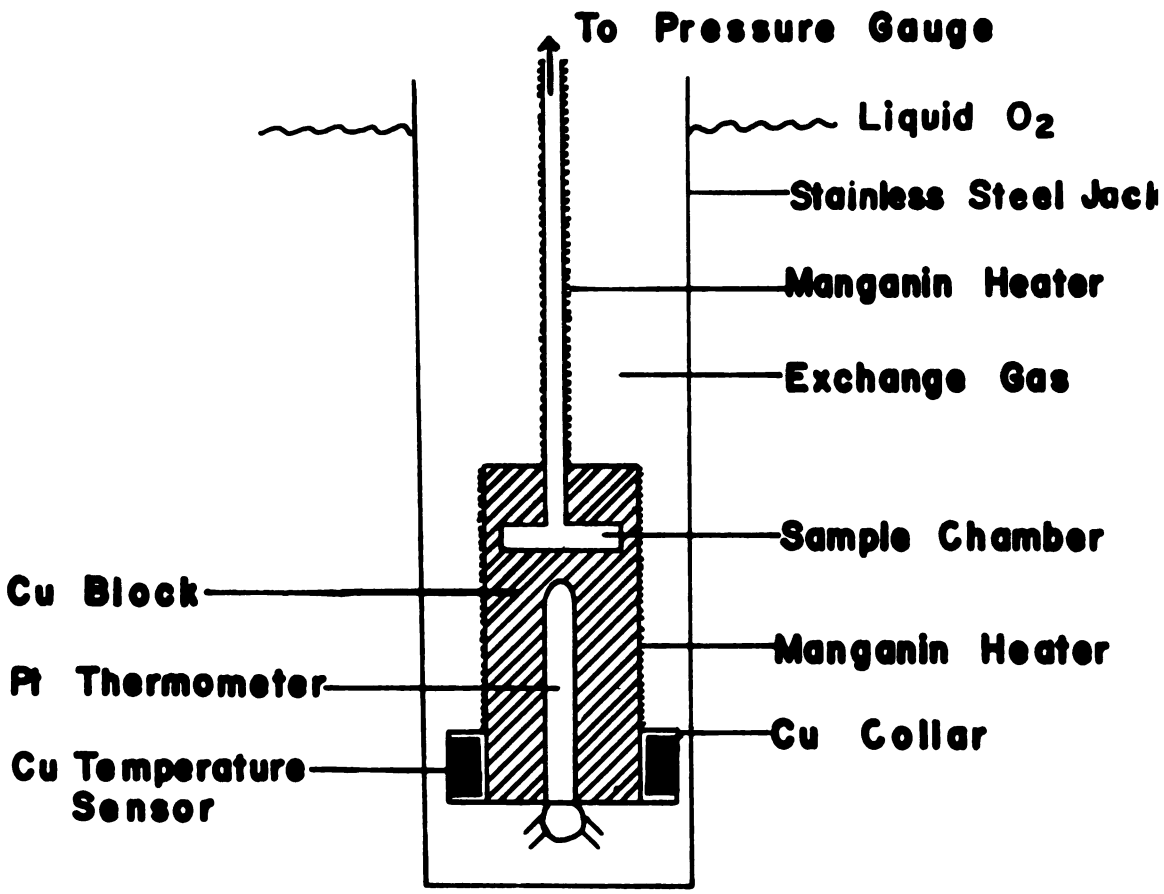

Figure 1: Sectional view of the cryostat used for this experiment.

heater wound on the tube. The tube was coated with cigarette paper and glyptal varnish to provide electrical insulation and to aid thermal contact of the heater and inlet tube. Power to this heater was supplied by a variable transformer.

A stainless steel outer jacket enclosed the Cu block. In order to allow the Cu block to be insulated from the liquid oxygen bath, the stainless steel jacket could be evacuated to a pressure of about 5×10^{-5} Torr. Electrical leads inside the stainless steel jacket were coated with Teflon to assure adequate electrical insulation. The leads exited from the top of the outer jacket through Kovar seals. The inlet tube was soldered in place at the top of the outer jacket and provided support for the Cu block containing the sample chamber.

Thermal contact between the sample chamber and the low temperature bath was achieved with He exchange gas. The gas was introduced into the stainless steel jacket directly from a He gas cylinder. In order to change the gas pressure, thus changing the thermal contact of the sample chamber and the bath, He gas was pumped away with a vacuum pump until the desired gas pressure was attained. The pressure of the He gas was measured with a Pirani gauge from 2 Torr to 0.01 Torr. Below 0.01 Torr a cold cathode ionization gauge was used to measure the He gas pressure.

Gas Handling and Sample Formation

The essential features of the gas handling system are shown in Figure 2. Pyrex was used to construct most of the system. Pyrex to Kovar seals were used to attach the glass system to the copper vacuum lines and to the stainless steel sample chamber inlet tube. High vacuum ground glass stopcocks were used throughout the system wherever valves were required. The stopcocks in this system were greased with Apiezon-L high vacuum grease.

An oil diffusion pump and nitrogen cold trap were used to evacuate the gas handling system. These pumps were capable of evacuating the system to about 4×10^{-6} Torr. While evacuating the system, pressures were measured on a cold cathode ionization gauge.

The ionization gauge sensor was located near the vacuum pumps as indicated in Figure 2. Because of the slow rate at which gases diffuse through the gas handling system at low pressures, the pressure in the remote parts of the system might have been slightly different than that measured by the ionization gauge. This possibility was checked by independently measuring the pressure using the McLeod gauge. The McLeod gauge was not highly accurate at the lowest pressures measured, but was accurate enough to indicate if the system had been evacuated throughout.

Originally the gas handling system was constructed of copper and brass. This system proved to be inadequate

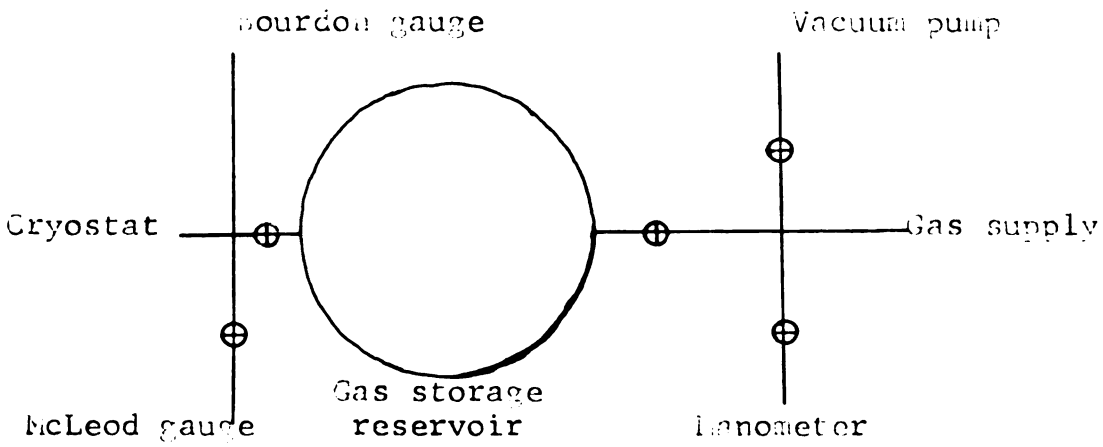

Figure 2: This drawing represents the gas handling system used in this experiment. The gas storage reservoir, vacuum lines, and stopcocks are shown.

because of outgassing of adsorbed materials from the surface of the metal. Even after heating and evacuating the system for a period of several hours, the pressure in the sealed-off system could be observed to increase at a rate of about 1 mTorr/hr.

After rebuilding the system, the gases adsorbed on the glass surfaces were removed by heating the system and evacuating the purged gases until no pressure increase could be observed. Following this degassing technique, the system could be sealed for several hours before any pressure increases were detectable. The system was always evacuated when not in use. Before each new gas sample was introduced, the system was heated for approximately 45 minutes to assure that adsorbed gases from the previous experiment were removed. The system was then sealed for several hours and the pressure monitored to guard against vacuum leaks or excessive outgassing.

Gas samples were transferred from metal storage cylinders to the gas handling system through a sealed stainless steel regulator. To estimate the number of moles of gas transferred to the system, the pressure of the gas in the system was measured on the mercury manometer. Since the total volume of the system was about 3500cm^3 and assuming that the gas followed the ideal gas law, the number of moles of gas in the system could be calculated. Immediately after the gases were

admitted, the manometer and regulator were sealed off in order to minimize contamination of the sample by mercury evaporated from the manometer.

All gas samples used were Matheson research grade gases. Mass spectrometer analyses provided with the samples listed the concentration of impurities. Table 4 shows the impurity concentration for the gases used in this experiment. More impurities may have been present because of outgassing from the walls of the storage cylinders.

TABLE 4

Impurity concentrations in gas samples used in this experiment. These tables are the results of a mass spectrometer analysis supplied with the gases.

(impurity)	(concentration)
Argon	
CO_2	less than 0.5 ppm
O_2	3.0 ppm
H_2	less than 1.0 ppm
CO	less than 0.5 ppm
N_2	less than 2.0 ppm
H_2O	3.5 ppm
CH_4	less than 0.4 ppm
Krypton	
N_2	2.0 ppm
O_2	1.0 ppm
Xe	13.0 ppm
Xenon	
N_2	2.0 ppm
Kr	18.0 ppm
O_2	1.0 ppm

After the system was filled with gas, the solid sample was carefully formed. Careful temperature measurement and control was necessary while condensing the sample in order to avoid condensation of gases on

the walls of the inlet tube.

In order to assure no condensation occurred on the inlet tube, the entire system was first electrically heated to a high enough temperature that gas could not condense. The stopcock which admitted gas from the gas storage reservoir to the sample chamber was then opened. Electrical heating was maintained on the inlet tube while the heating of the Cu block was slowly decreased. This assured that the block was the coldest part of the system.

While lowering the temperature of the Cu block, the pressure reading on the Bourdon gauge was monitored. When the sample began to condense, the gas pressure began to drop. By lowering the temperature slowly, the gas pressure remained near the equilibrium vapor pressure as the sample was formed. Because gases only condense on surfaces where the gas pressure is higher than the equilibrium vapor pressure, slow condensation assured that condensation occurred only in the coldest part of the system.

Samples were condensed at various temperatures. The ultimate vapor pressure data did not depend on the initial condensation temperature. Three distinct methods were used for condensation of the samples.

In the first method, samples were condensed above the triple point temperature so that the gas condensed into the liquid phase. The liquid rare gas was then

slowly frozen and the sample was used for measurements.

The second method consisted of condensing the sample at temperatures below the triple point. In this case, the gas was condensed directly into the solid phase.

In the third method, samples were condensed as in the second method; however, after condensation the samples were annealed near their triple points in order to increase the grain size of the polycrystalline sample.

According to previous studies of crystal growth of the rare gases,[26] the different growth rates of each of these techniques produces different average grain sizes in the solid formed. No change in vapor pressure data was observed which depended on the technique used to form the sample. Therefore, it was concluded that vapor pressure is not a function of grain size.

Another effect which was investigated was the possible change in vapor pressure due to preferential evaporation at grain boundaries.[27] It is known that rare-gas solids show thermal etching at grain boundaries. However, it is not known if the etched lines result from preferential evaporation or from surface migration away from grain boundaries. If thermal etching is a result of preferential evaporation, there is a possibility that the vapor pressure of a newly formed sample might be higher than the vapor pressure of a solid which has already undergone thermal etching.

By observing the variation in pressure with time, it was found that the pressure of the solid sample

reached equilibrium in a short time after crystal growth stopped. The sample was then maintained at a constant temperature for up to an hour and no further measurable pressure changes were observed. Because no measurable pressure changes occurred, it was assumed that if preferential evaporation were responsible for thermal etching, the expected change is too small to be observed.

The volumes of the condensed samples were approximately $0.8cm^3$. In order to estimate the sample volume, the number of moles of gas condensed was determined. Using the Bourdon gauge, the pressure change in the gas storage reservoir was measured as the sample was condensed. Knowing the volume of the gas storage reservoir ($3500cm^3$) and assuming the ideal gas law applies, the number of moles condensed was calculated. By using accepted densities of rare-gas solids[2], it was then possible to calculate the volumes of the condensed samples.

After the samples were formed, the system was checked for parasitic condensation of gases on the walls of the inlet tube. This was done by maintaining the sample temperature constant and increasing the current to the inlet tube heater. If the pressure was observed to increase under these conditions, it was assumed that gases had condensed on the walls of the inlet tube. It was found that if gases were condensed

on the inlet tube, the entire sample had to be evaporated and replaced before taking data.

After condensation the sample was distilled *in situ* to lower the concentration of non-condensable impurities. Distillation was accomplished by first lowering the sample temperature until almost all of the primary gas component was condensed. The gas storage reservoir was then evacuated to the lowest pressure attainable, about 6×10^{-6} Torr. After evacuation, the gas storage reservoir was first sealed off from the vacuum pump by closing the stopcock. The gas storage reservoir was then opened to the sample chamber and the vapor above the sample chamber expanded into the evacuated gas storage reservoir. After this expansion the gas storage reservoir was again sealed off from the sample chamber, opened to the pump, and evacuated. This technique assured that most of the vapor phase which contained the non-condensable impurities was removed and discarded. After the distillation, pure vapor sublimed from the solid and replaced the impure vapor which had been removed. After successive distillations caused no further change in the measured sublimation pressure, data were taken using the purified sample.

Temperature Control

Many techniques exist for accurate temperature regulation of cryostats. Some control may be achieved by simply immersing an experiment in a cryogenic bath

and controlling the bath temperature. However, this technique is of limited value because suitable cryogenic baths only exist over narrow temperature ranges. Also the problem of accurately controlling bath temperature over wide ranges is difficult.

In order to provide more reliable control and to expand the range of available temperatures, electrical heating may be applied. The type of electrical temperature controller used depends on the application. For example, in adiabatic calorimeters, the heat input requirements are quite stringent so that control systems are employed which minimize the amount of heating applied directly to the sample.

In order to attain the temperatures desired for our experiment, a combination of methods was employed. For temperatures from 90 - 55K the apparatus was immersed in a liquid oxygen bath. The bath temperature was lowered by controlling the vapor pressure above the liquid with an automatic pressure regulator.

The pressure regulator could maintain the vapor pressure of the liquid stable to about $\pm$ 0.1 Torr. This permitted control of the bath temperature to about $\pm$0.02K over most of the range between 90 - 55K. Temperature of the bath was determined from vapor pressure measurements made with a mercury manometer. Accepted vapor pressure tables[28] were used to calculate the temperature from these pressure measurements.

When temperatures above 90K were required, the Cu block containing the sample chamber was thermally insulated from the liquid oxygen bath by removing the He exchange gas. Electrical heating was then applied to the Cu block by means of the manganin wire heater wound on the block. The amount of electrical heating was regulated to produce the desired temperature.

To achieve temperatures below 55K the apparatus was suspended above a liquid He bath while cold vapor was evaporated from the bath and pumped around the outer stainless steel jacket. In order to produce the desired temperature, it was necessary to carefully vary the exchange gas pressure and the rate of evaporation from the liquid He bath.

The techniques described were used to attain the temperatures desired. However, none of these techniques quite provides a reliable and convient method of controlling the cryostat temperature with sufficient accuracy. More carefully controlled electrical heating was needed to maintain the temperature stability within the tolerances required for accurate results. This controlled electrical power was supplied to the manganin heater, which was on the Cu block, by means of a Model 1053, Hallikainen Instruments, Thermotrol ac bridge temperature controller.

In principle an ac bridge temperature controller consists of a Wheatstone bridge circuit driven by an

ac voltage source. The bridge circuit is connected to an amplifier to supply power to a heater as shown in Figure 3. One arm of the bridge is temperature sensitive and is thermally anchored to the Cu block containing the sample chamber. A change in the temperature of the sensitive arm of the bridge produces an unbalanced condition in the bridge. The signal from the unbalanced bridge is then phase analyzed to determine whether the controller should increase or decrease its power output. If a power increase is required the out-of-balance signal from the bridge is amplified and supplied to the heater.

The temperature controller used in this experiment supplied pulses of power to the heater. Power of the pulses supplied to the Cu block matched the thermal losses to the bath. When the bridge circuit became unbalanced, the duration of the pulses changed to return the system to thermal equilibrium.[29]

A resistive temperature sensor of 40 gauge Cu wire served as the temperature sensitive arm of the bridge. The wire was wound non-inductively on a Cu collar which was placed around the Cu block containing the sample chamber. Room temperature resistance of this sensor was approximately 300Ω .

Copper thermometers are not normally used for low-temperature measurements because their resistivity is not reproducible over several cooling cycles. However,

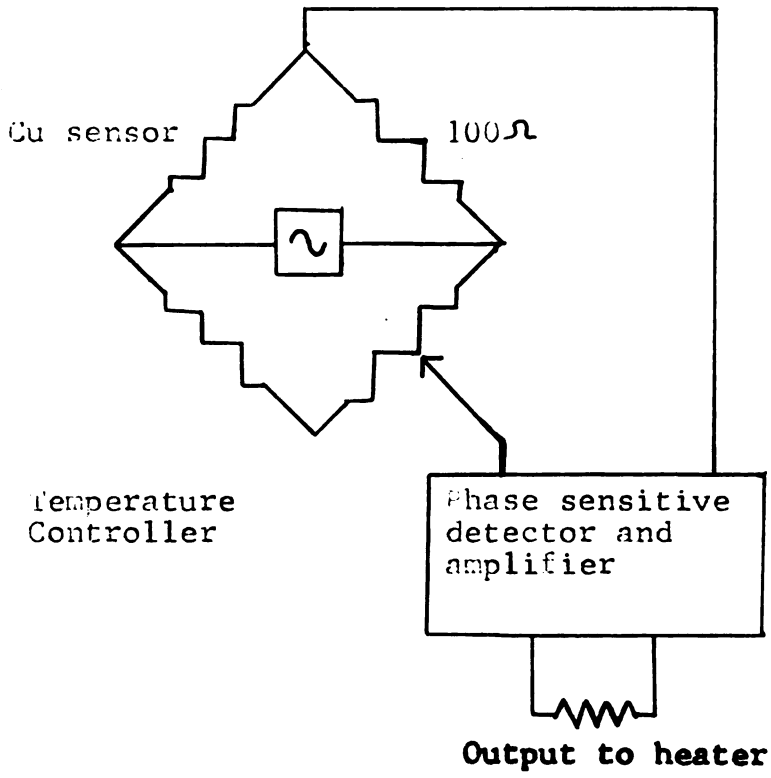

Figure 3: The operation of the ac bridge temperature controller is indicated in this schematic drawing.

the resistivity changes rapidly with temperature above about 20K so that such a thermometer is quite sensitive to temperature changes. It is this latter condition which is important when the thermometer is used as a sensor to detect small temperature changes. Thus copper makes a good sensor for a temperature controller but cannot be reliably calibrated for absolute temperature measurements.

The output of the temperature controller was supplied to the 1250Ω manganin heater wound on the block containing the sample chamber. A layer of cigarette paper coated with glyptal varnish was placed between the copper block and the heater in order to assure electrical insulation and to improve thermal contact between the copper block and the heater. Series resistors varying from 100Ω to 4700Ω were attached in series with the manganin heater to reduce the amount of power supplied to the heater.

When the copper block temperature was nearly in equilibrium with the bath, only small amounts of electrical heating were necessary to maintain temperature control. It was found that by reducing the amount of power to the heater by means of series resistors, more stable control was achieved. Improved control resulted because the pulses of power directly from the controller were large enough to cause temperature oscillations in the Cu block due to the alternate heating and cooling as pulses

were applied. By reducing the amount of power supplied to the Cu block with each pulse, the size of the temperature oscillations between pulses was greatly reduced.

With this system it was possible to control the sample temperature to ± 1 mK for the length of time necessary to take measurements and to ± 5 mK for longer periods of time. Some slow drifts of sample temperature were observed due to changes in room temperature.

Temperature Measurement

The sample temperature in this experiment was measured using platinum resistance thermometers. Resistance of the thermometers was measured using a potentiometer.

Two different thermometers were used to measure temperature in this experiment. Calibration of these thermometers was supplied by the National Bureau of Standards. These calibrations were based on the 1968 International Temperature Scale for which the following relations apply: triple point temperature of water = 273.16K = 0.01°C, and boiling point temperature of oxygen = 90.188K = -182.962°C.[25]

The thermometers used were four-lead Model 8164 Leeds and Northrup capsule-type Pt resistance thermometers. For measurements below 91K we used the thermometer with serial number 1644176. The thermometer used for measurements above 91K had serial number 1737395.

When data were taken, the thermometer in use was imbedded in the Cu block as shown in Figure 1. If it was

desired to use a different thermometer, the apparatus was brought to room temperature, the outer stainless steel jacket removed, and the thermometer in use was replaced.

Thermal contact between the Cu block and the resistance thermometer was aided by a thin layer of Apiezon-L vacuum grease. The thermometer leads were thermally anchored to the surface of the Cu block.

In order to assure that the sample and the thermometer were at the same temperature, the existence of thermal gradients in the Cu block and in the sample was investigated in the following way. The pressure of the exchange gas in the vacuum space around the Cu block was increased to improve the thermal contact of the Cu block and the He bath. Electrical heating from the temperature controller was simultaneously increased to maintain the block temperature constant. The vapor pressure reading was monitored to insure that no change in sample temperature occurred when heater power was increased. This technique is capable of detecting changes in sample temperature of less than 1 mK.

Small thermal gradients of about 2 mK were observed when the heater power input approached its maximum value, 10 watts. In order to minimize these thermal gradients, the heater was never operated above about 10% of maximum power when taking data.

Thermal gradients due to the heater on the inlet tube were similarly investigated; however, none were detected. In this case the temperature of the Cu block measured with the Pt thermometer was held constant while the power to the inlet tube heater was varied. Although it was observed that heat was conducted into the Cu block from the inlet tube, no measurable thermal gradients were observed in the block.

Thermometer resistance was measured using a Leeds and Northrup calibrated K - 5 guarded potentiometer using a single-potentiometer technique.[31] The null detector used was a Leeds and Northrup Model 9834. All parts of the measuring circuit were guarded to prevent error due to leakage currents.

Potentiometer readings have an estimated accuracy of $\pm$ 0.2 μV. The potentiometer calibration was certified by the manufacturer. It was reported that no corrections were necessary in order to assure readings within the desired accuracy.

A schematic representation of the temperature measuring circuit is shown in Figure 4. The four platinum leads from the thermometer were soldered to terminals attached to Cu leads from the potentiometer system. Two of the leads supplied current from a 6.0V lead-acid cell to the thermometer windings. Thermometer current was controlled by a ten-turn potentiometer used as a shunt across a 100 Ω resistor. The voltage drop

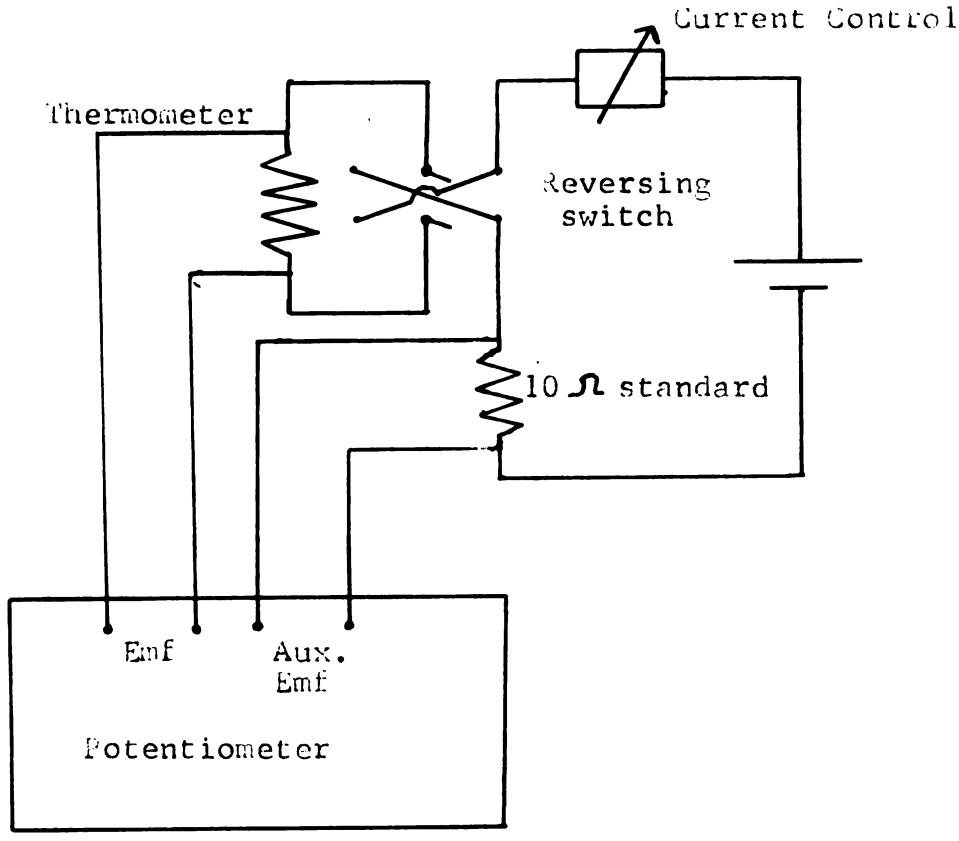

Figure 4: This potentiometer circuit was used for temperature measurement. Current to the thermometer was reversed to account for thermal emfs in the system.

across a 10 Ω standard resistance in series with the thermometer and lead-acid cell was measured on the "Auxiliary Emf" scale of the potentiometer. This measurement was used to determine the thermometer current.

For measurements below 90K the current through the thermometer was maintained at 2.0 mA. These currents corresponded to the currents applied when the respective thermometers were originally calibrated. These currents were controlled and measured to within $\pm 0.05 \mu$A.

The potential drop across the resistance thermometer was measured on the "Emf" terminals of the potentiometer. By using a potentiometer, lead resistances may be ignored in these measurements. No current flows through the thermometer leads when the potentiometer is balanced.

Although lead resistances do not affect measured voltages, the effect of thermal emfs must be eliminated from all measurements. Thermal emfs were minimized in the measuring system by using continuous Cu leads from the resistance thermometer to the potentiometer terminals. However, even with this precaution, thermal emfs as large as 4 μV were sometimes present in the measuring circuit.

In order to compensate for the effect of these thermal emfs, the direction of the current through the thermometer was reversible. For each temperature

determination, two potential measurements were made with the current reversed between measurements. The first measurement was taken using the potentiometer in the "Emf" setting. The current was then reversed and readjusted to the proper value. Finally, a second potential reading was taken using the "Reverse Emf" setting of the potentiometer.

The difference in these two potential measurements is twice the value of the thermal emfs present. The average value of the two readings is equal to the potential drop across the resistance thermometer.

Care was taken to eliminate random errors due to changes in thermal emfs as the sets of potentiometer measurements were being made. All terminal posts and lead wire connections were thermally insulated to reduce temperature fluctuations at connections where thermal emfs might be present. For each data point, six to eight pairs of potential measurements were made. This assured that the size of thermal emfs was remaining constant. If rapid changes in thermal emfs were observed, the measurements were repeated when the thermal emfs reached equilibrium.

Temperature measurements made using the techniques described above have an estimated sensitivity of approximately $\pm$ 0.5 mK. The sensitivity is reduced at low temperature due to the decreased sensitivity of the resistance thermometer. Absolute temperature accuracy depends on

accuracy of the thermometer calibration and potentiometer calibration. Assuming negligible error in the thermometer calibration, the absolute accuracy of voltage measurements permits temperature measurement to within $\pm$2 mK.

Pressure Measurement

Vapor pressure was measured over eight orders of magnitude in this experiment. Because of the wide range of pressures measured, different techniques and corrections were applied depending on the pressure range being considered.

Pressures above 1 Torr were measured using a Texas Instruments Model 142 quartz spiral Bourdon gauge. Basically this gauge consists of a fused quartz Bourdon tube and a readout device to measure the tube deflection.

Deflection of the Bourdon tube is measured optically. Light is reflected from a mirror attached to the end of the Bourdon tube. The reflected light beam is located by means of a photocell. The Bourdon tube is calibrated to determine the relation between the angle of deflection and the pressure.

For this experiment two Bourdon tubes were used which covered pressures from 0 - 250 Torr and 250 - 500 Torr, respectively. The photocell detector was attached to a counter which divides the full scale deflection into 300,000 counts. Thus the full scale deflection of 250 Torr was divided into 300,000 counts resulting in a

gauge sensitivity of better than 1 mTorr.

At low pressures oscillations of the Bourdon tube which were driven by vibrations present in the room were sometimes observed. The entire system was isolated from vacuum pumps and other sources of vibrations to eliminate these oscillations. At high pressures, vibrations presented only minor problems because damping was supplied by the gases in the Bourdon tube.

The reference space surrounding the Bourdon tube was evacuated to 10^{-5} Torr by means of an oil diffusion pump. It was possible to admit air into the reference space in order to damp vibrations which were sometimes started by accidental shocks to the system. Small amounts of air in the reference space could damp vibrations and could then be evacuated before pressure measurements were made.

The Bourdon gauge was calibrated using a Hg manometer read with a Wild cathetometer. The manometer was constructed from 12mm i.d. glass tubing. Before being filled with mercury, the manometer was carefully cleaned with commercial glass cleaner and then with dilute nitric acid. The manometer was then rinsed with distilled water followed by methanol. The methanol was then evaporated by means of a vacuum pump.

After being cleaned, the manometer was filled with reagent grade mercury. When not in use the manometer was evacuated to prevent oxidation of the mercury.

Using the cathetometer, the mercury level of the manometer could be determined to within ±0.02mm. However, corrections were applied to these readings to account for capillary depression of the mercury.[32] For each pressure reading the height of the mercury meniscus was recorded and the tables in reference 32 were used to calculate capillary depression of each reading.

In order to eliminate the effect of thermal expansion of the mercury, the manometer readings were then corrected to correspond to 0°C density of mercury. Care was taken to keep the temperature of the manometers stable while the calibration was being made. Room temperature was measured and the mercury density was corrected using accepted tables of mercury density.[33]

Manometer readings were also corrected to correspond to readings taken under conditions for standard gravitational attraction. For standard gravitational attraction, $g = 980.665$ cm/sec^2. The accepted value for local gravitational attraction in our laboratory was, $g = 980.350$ cm/sec^2.

The effect of the combined corrections to adjust the manometer readings to 0°C density of mercury and standard gravity was to introduce a factor which made the corrected mercury level lower than the actual mercury level. These corrections never exceeded 0.5%.

The absolute accuracy of the Bourdon gauge calibration using the manometers described above is ±0.02 Torr.

Because the gauge response was nearly linear over narrow pressure ranges, the gauge can be used to measure accurately small pressure changes to within $\pm$ 2m Torr.

Below 1 Torr pressures were measured using a Consolidated Vacuum Corporation Type GM-100-A McLeod gauge. Calibration of this gauge was supplied by the manufacturer. The McLeod gauge readings agreed with the manometer below 1 mm to within the limits of error of the manometer readings. The McLeod gauge was welded into the glass vacuum system connecting the gauge to the sample chamber. When not in use the gauge was evacuated and sealed from the rest of the system by means of a high-vacuum stopcock.

Before data were taken, the McLeod gauge was degassed by heating and evacuating the gauge. Degassing was necessary not only to prevent contaminants from reaching the sample chamber but also to prevent sticking of the mercury column in the gauge capillaries.

A cold trap separated the McLeod gauge from the sample chamber. The cold trap prevented contamination of the sample by mercury diffusing from the McLeod gauge. A bath of dry ice and acetone was used to refrigerate the cold trap. This mixture produced a bath temperature of 200K which was cold enough to condense gaseous mercury but was warm enough to prevent condensation of rare gases.

All McLeod gauge readings were corrected for mercury streaming.[34] Because of the flow of mercury vapor from the McLeod gauge to the cold trap, the pressure in the McLeod gauge is reduced. This process is similar in principle to the operation of a diffusion pump. The diffusing vapors collide with gas molecules and impart momentum in the direction of diffusion. This causes a pressure gradient between the McLeod gauge and the cold trap which can be calculated from the equation,[34]

$$\ln P[(\text{Real})/P(\text{McLeod})] = .905\ r\ P_{Hg}(T^{\frac{1}{2}}/D_{12}) \quad . \quad (37)$$

In equation (37), r is the radius in cm of the tube connecting the McLeod gauge with the pressure to be measured, T is the room temperature in Kelvins, D_{12} is the diffusion coefficient in cm^2/ sec at 1 atmosphere and 300K for the gas in the gauge diffusing into Hg vapor, and P_{Hg} is the vapor pressure of mercury in Torr at room temperature.

Accepted values for the vapor pressure of mercury were used for these calculations.[35] Values used for diffusion coefficients are[34]: for Ar, D = 0.12 cm^2/sec; for Kr, D = 0.093 cm^2/sec; for Xe, D = 0.079 cm^2/sec. The radius of the tube connecting the McLeod gauge with the pressure to be measured was, r = 0.3 cm. Using these values the correction never exceeded 10% of the McLeod gauge reading.

Near 1 Torr, the McLeod gauge readings have an estimated accuracy of 1%. Between 10^{-4} - 10^{-5} Torr,

the lower usable limit of the gauge, the gauge readings are estimated to be accurate to within 5%. Additional error may be present due to inaccuracy in the diffusion coefficient values used for the mercury streaming correction. This error could be as much as 1%.

Readings below 1 Torr were also corrected for thermal transpiration. This effect is observed when two vessels connected by a narrow tube are kept at different temperatures. When the pressure of the gas in the vessels is low enough that the mean free path of the gas molecules is several times the diameter of the connecting tube, it is found that the pressure is higher in the warmer vessel. The ratio of the pressures for this case may be simply expressed as $P_1/P_2 = \sqrt{T_2/T_1}$.[36] Here, P_2 and P_1 are the pressures in the respective vessels and T_2 and T_1 are their absolute temperatures.

If the mean free path of molecules in the gas is short compared to the diameter of the connecting tube, no pressure gradient is observed.

However, for most actual pressure measurements, the mean free path of the gas molecules is between the two extremes. In this case, the ratio of pressures in the two vessels may be calculated from the empirical equation,[37]

$$\frac{P_1}{P_2} = \frac{\sqrt{T_1/T_2} - 1}{A^* X^{*2} + B^* X^* + C^* \sqrt{X^*} + 1} + 1 \quad , (38)$$

where $T_2 > T_1$ and $X^* = 2 P_2 d/T_1 + T_2$.

In equation (38), P_2 represents the pressure measured at room temperature, T_2, and P_1 represents the pressure of the sample in the cryostat at temperature, T_1. The parameter d is the diameter in mm of the tube connecting the sample and the room temperature pressure gauge. For this experiment the value of d was 6.35 mm.

The values of the parameters A^*, B^*, and C^* depend on the gas which is being used for pressure measurements. Table 5 shows the values A^*, B^*, and C^* used for this correction.[37]

TABLE 5

Values of the parameters A^*, B^*, and C^* of equation (38).

Gas	$A^*(10^5 K^2/Torr^2\ mm^2)$	$B^*(10^2 K/Torr\ mm)$	$C^*(K^{\frac{1}{2}}/Torr^{\frac{1}{2}} mm^{\frac{1}{2}})$
Ar	10.8	8.08	15.6
Kr	14.5	15.0	13.7
Xe	35	41.4	10

This correction appeared to be adequate for pressures above about 0.1 Torr. At this pressure, the sample pressure was approximately 20% lower than the pressure measured at room temperature.

For lower pressures, deviations appeared which could only be attributed to the correction. The vapor pressure parameters presented in Table 11 have anomalously low values for reduced temperatures between 0.7 and 0.5. These values indicate a large overcorrection in this range. Deviations probably occur at lower pressures

also but are masked by other effects. This correction for thermal transpiration becomes unreliable at low pressures but no adequate correction is available.

IV. RESULTS

The measured pressure and temperature points are presented in Table A1, Table A2, and Table A3 in the Appendix. Figures 5, 6, and 7 of the text show the measured sublimation pressures, P, plotted as functions of the temperature, T, for Ar, Kr, and Xe, respectively.

Law of Corresponding States

The sublimation pressure curves of rare-gas solids may be related by means of the law of corresponding states.[38] As discussed earlier, the reduced equation of state for rare-gas solids should depend only on the reduced temperature, T^*, the reduced volume, V^*, and the reduced de Broglie wavelength Λ^*. Thus, for all the rare-gas solids the reduced sublimation pressure curve is given by equation (14).

It is further expected that the reduced sublimation pressure curves should increase monotonically with increasing Λ^*.[39] The parameter Λ^* defined by equation (10), indicates the relative size of quantum effects in the crystal.

Physically, a large value of Λ^* represents a crystal with large reduced zero point energy, E_z^*. Because the reduced zero point energy is larger for

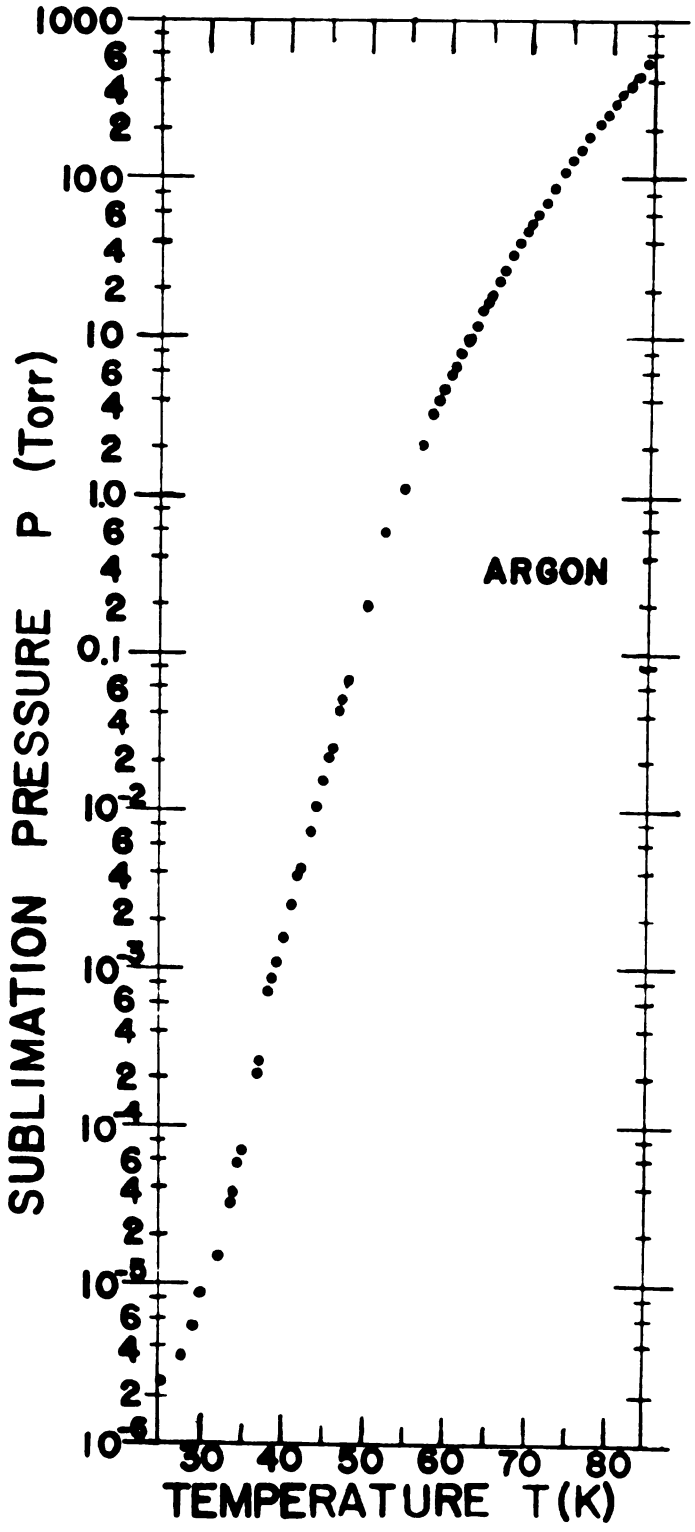

Figure 5: Measured sublimation pressures are plotted for Ar.

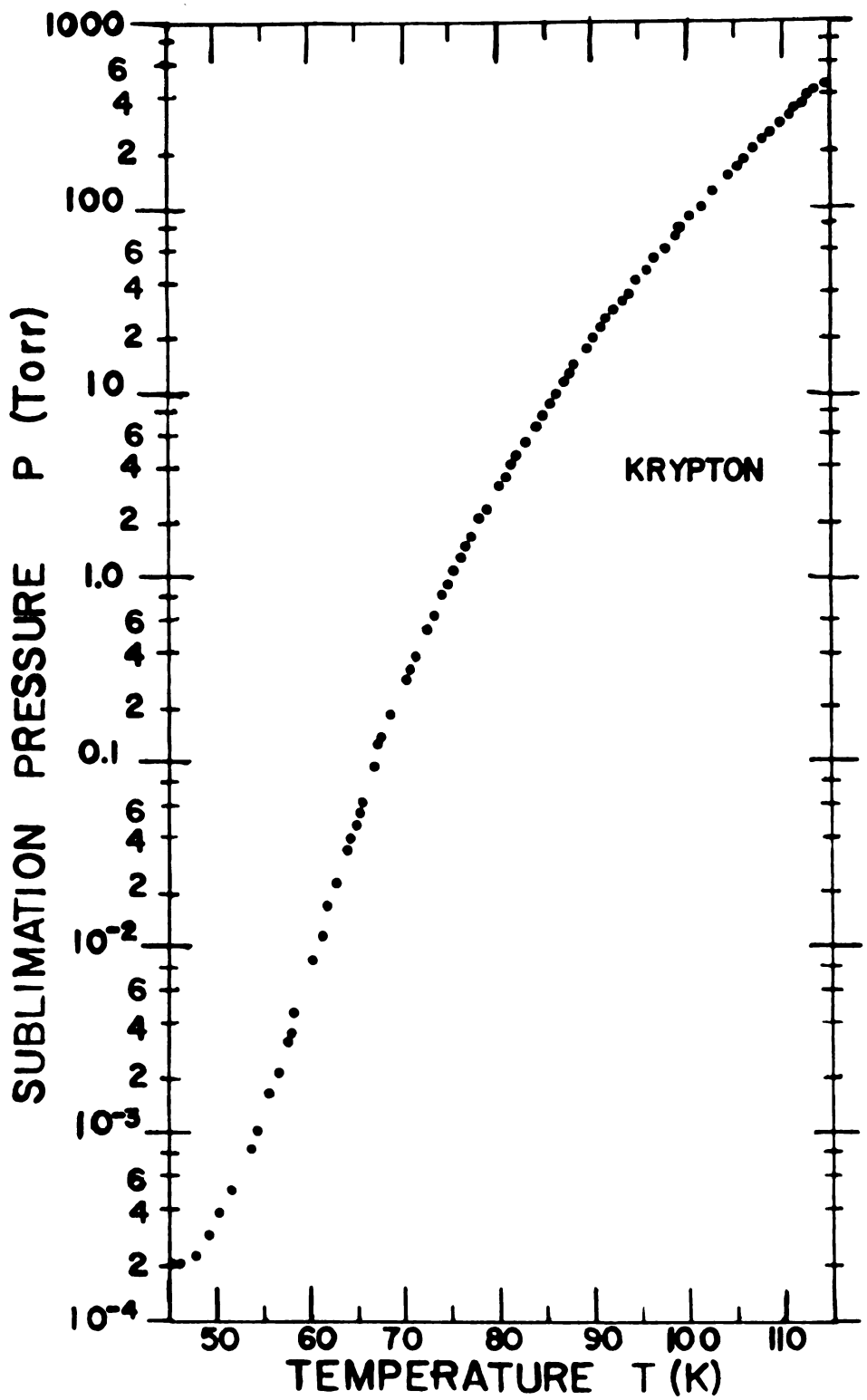

Figure 6: Measured sublimation pressures are plotted for Kr.

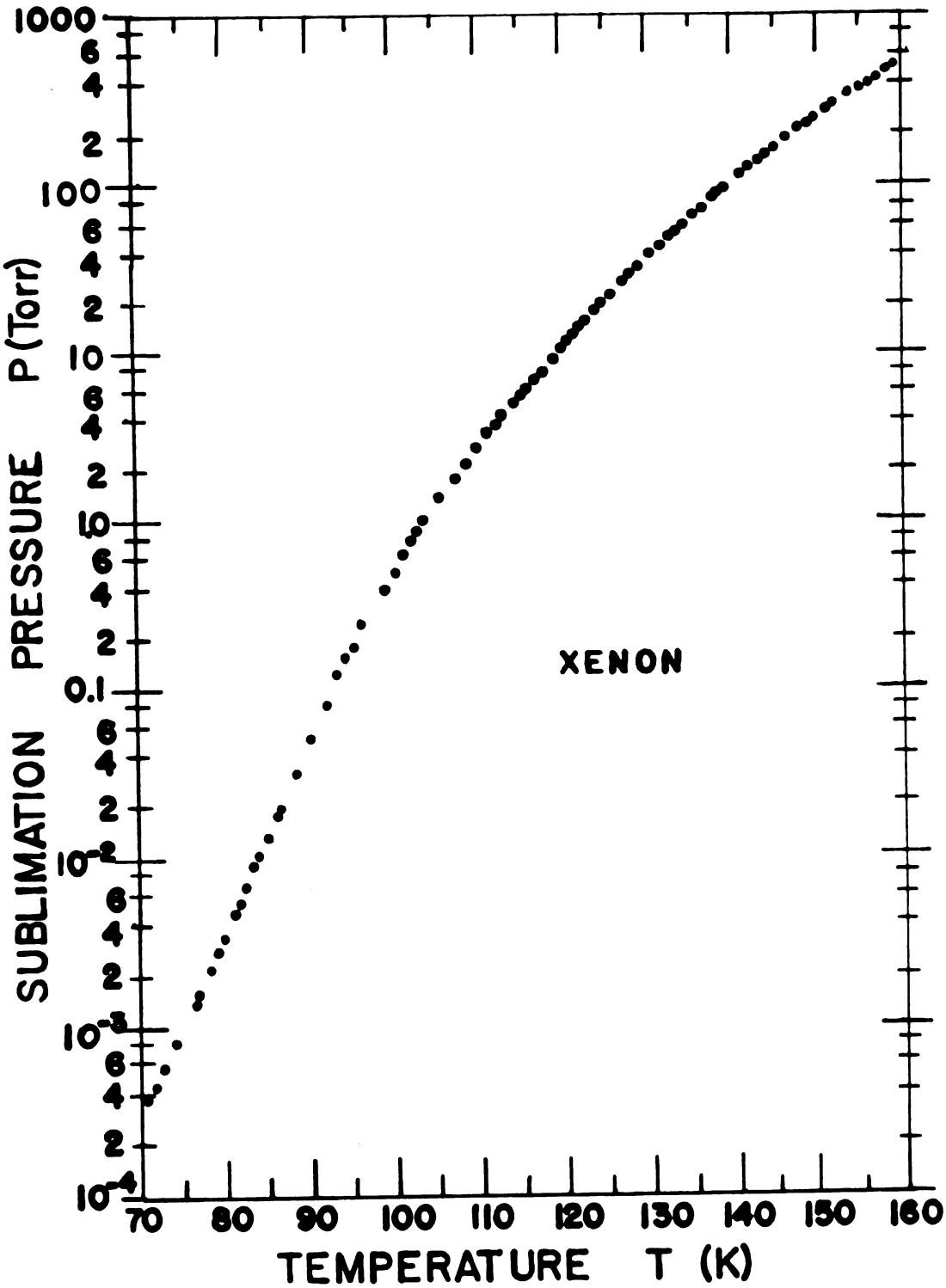

Figure 7: Measured sublimation pressures are plotted for Xe.

solids with large values of Λ^*, the molecules are more easily removed from the lattice. Hence, the larger the value of Λ^*, the higher the expected reduced vapor pressure.

Values for Λ^* found using the all-neighbor Mie—Lennard-Jones potential are presented in Table 3. Because Λ^* is larger for Ar than for Kr and Xe, the reduced vapor pressure curve for Ar should lie above the curves for Kr and Xe, respectively. Using the potential parameters of Table 3 the reduced pressure curves were plotted using data from this experiment. These curves deviate from the expected order as can be seen in Figure 8.

The reduced pressure curves lie close together as expected. However, the Kr and Xe curves are interchanged from the predicted order. This effect has been observed in other properties and by other investigators.[38,39]

The reasons for this deviation are not clear. In the pressure range considered, the deviation is larger than the expected error in the vapor pressure data. Because all the data were taken using the same apparatus, the effects of systematic error should not change the relative position of the curves.

Another possible reason for the inversion of order is the inaccuracy in the determination of the potential parameters ϵ and σ. A change of only 2-3% in the values of ϵ and σ would reverse order of the Kr and Xe curves. The stated error of the values of ϵ and σ

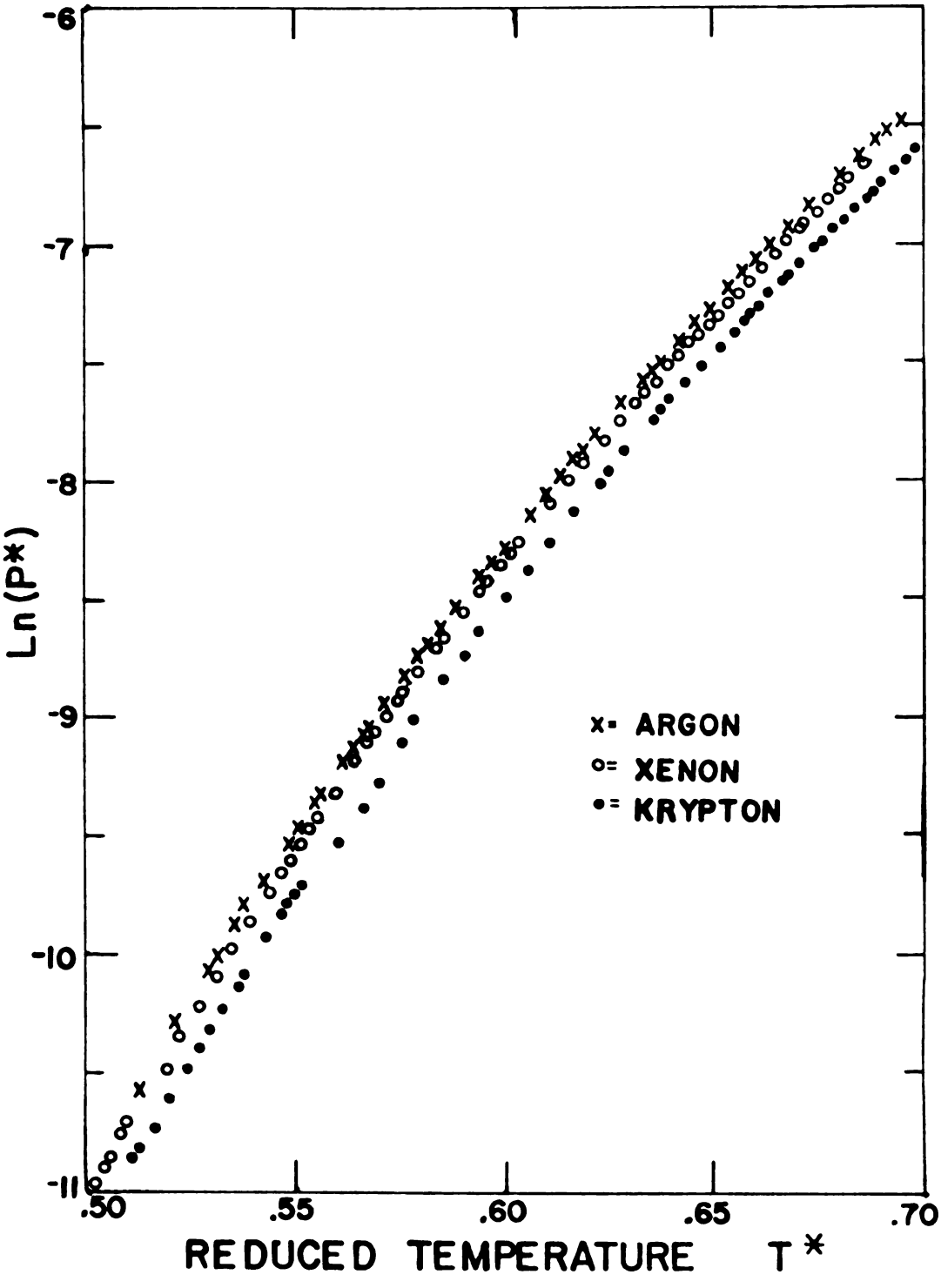

Figure 8: Reduced sublimation pressure curves are plotted for Ar, Kr, and Xe.

is less than the amount required to change the order of the Kr and Xe curves.[3] However, it is likely that the actual potential deviates from the analytic Mie—Lennard-Jones potential for which ϵ and σ were determined. Thus, the values of ϵ and σ for the Mie—Lennard-Jones may differ from the parameters for the actual potential. Although the Mie—Lennard-Jones potential has the necessary form, $\phi(r) = \epsilon f(r/\sigma)$, the accepted values of ϵ and σ only represent the values which make the shape of the calculated potential as much as possible like the shape of the actual potential.

Static Lattice Energy

By applying equation (30) to the data of this experiment, the static lattice energy, E_o, and the geometric mean of the lattice vibrational spectrum, ω_g, could be determined for Ar, Kr, and Xe. As described earlier, the quantities E_o and ω_g may be determined from a plot of $\ln PT^{\frac{1}{2}}$ versus $1/T$. P is the measured sublimation pressure and T is the sample temperature. Typical plots of the data for Ar, Kr, and Xe are shown in Figures 9, 10, and 11, respectively. The slope of each plot yields E_o and the intercept yields ω_g.

In practice however, it was found that more accurate results could be obtained by fitting the data to equation (30) by using the method of least squares. Equation (30) is first linearized into $y = a + bx$

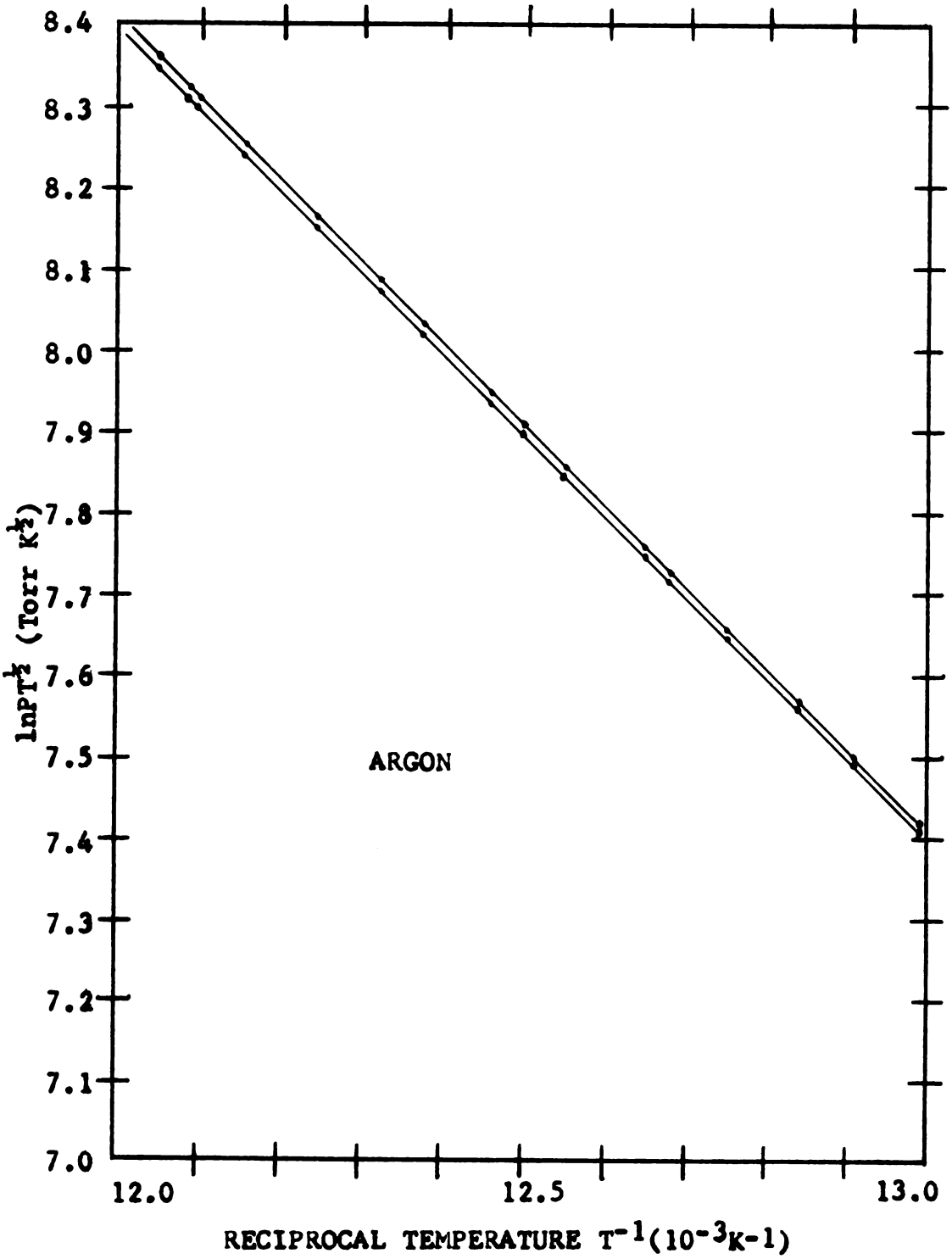

Figure 9: Typical plot of $\ln PT^{\frac{1}{2}}$ versus 1/T for Ar. Upper line is corrected for vacancy formation.

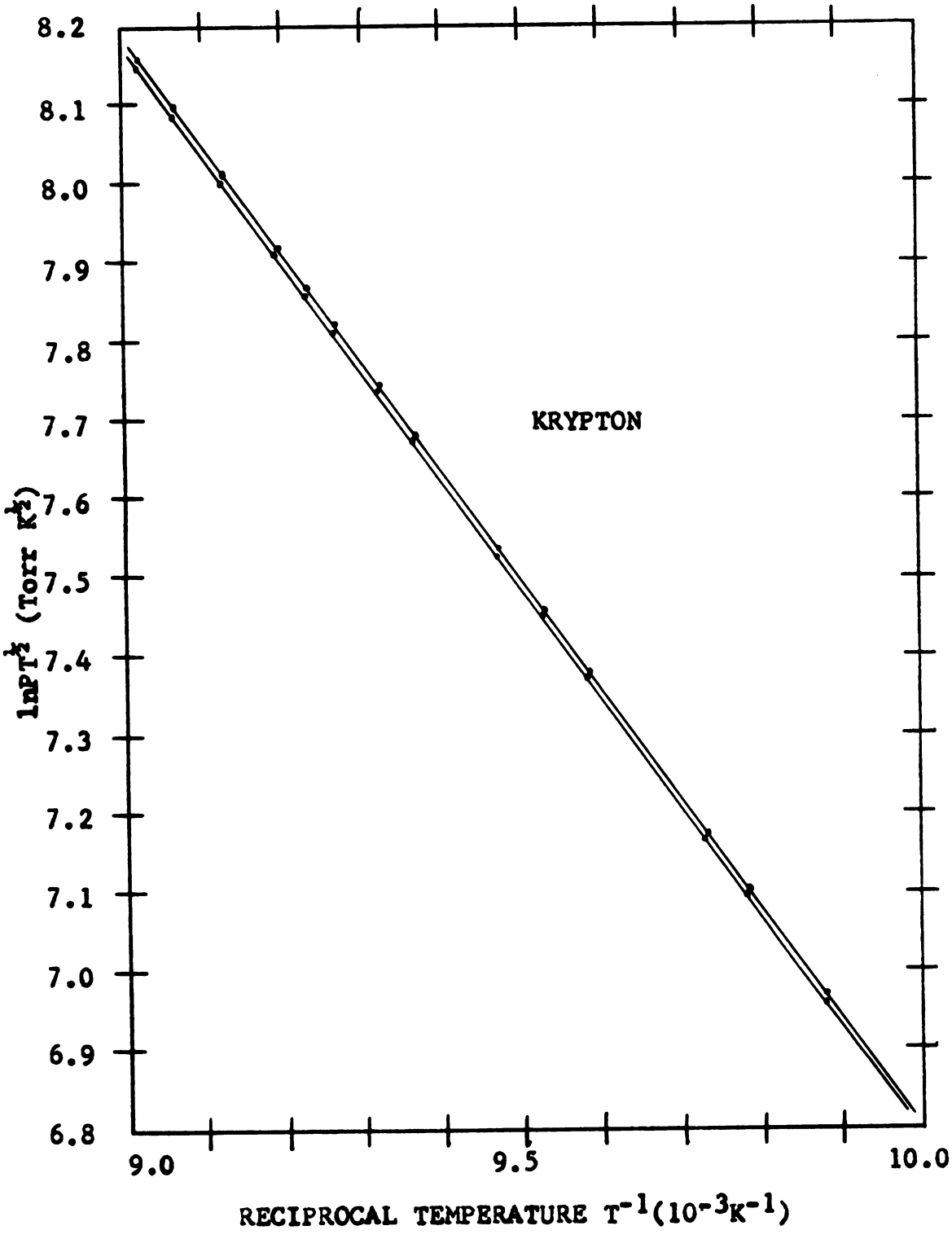

Figure 10: Typical plot of $\ln PT^{\frac{1}{2}}$ versus 1/T for Kr. Upper line is corrected for vacancy formation.

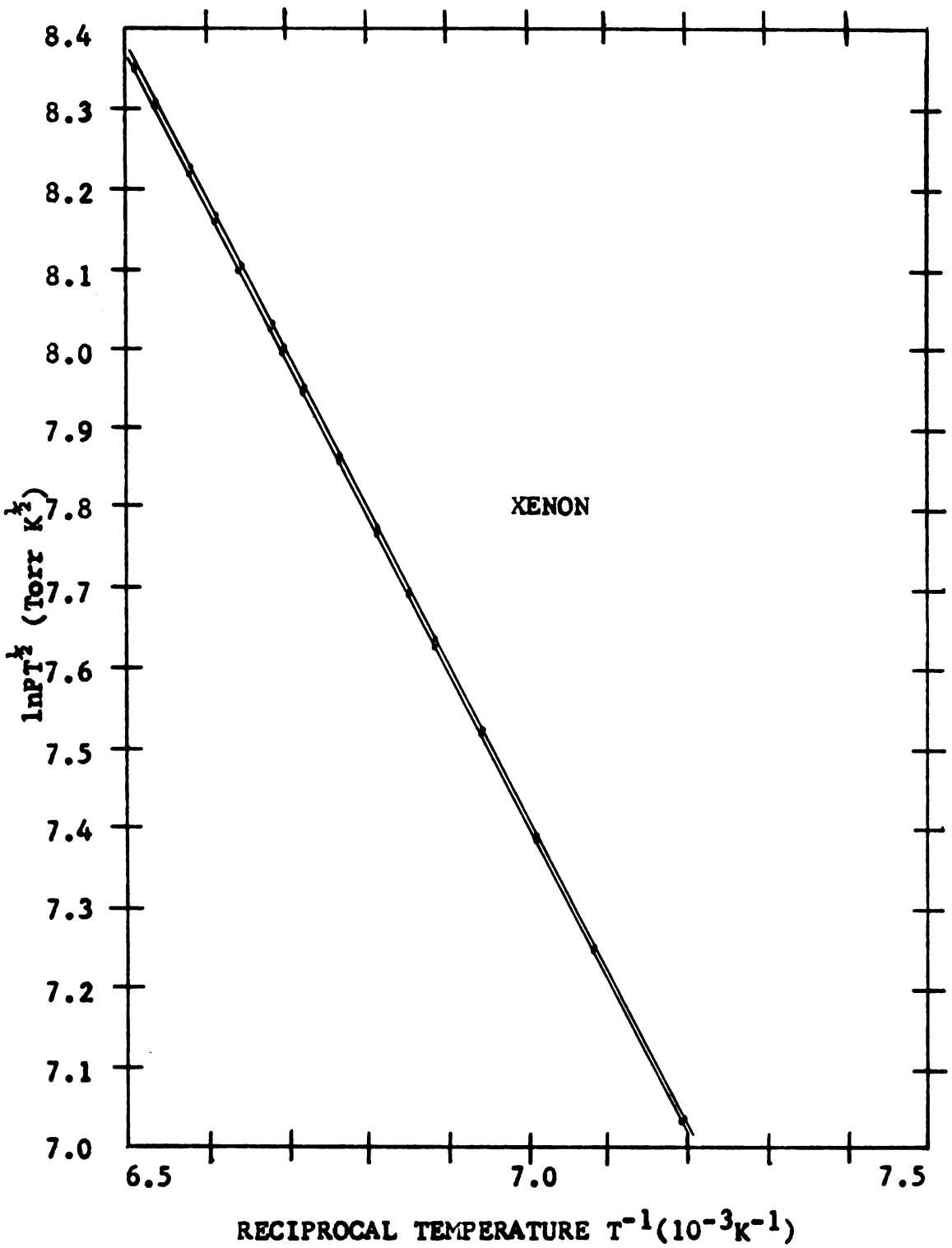

Figure 11: Typical plot of $\ln PT^{\frac{1}{2}}$ versus 1/T for Xe. Upper line is corrected for vacancy formation.

where $y = \ln PT^{\frac{1}{2}}$ and $x = 1/T$. Then using the standard method for linear regression, a and b can be determined from the equations[40]:

$$a = \left(\sum_i y_i - b \sum_i x_i \right) / n$$

$$b = \frac{n \sum_i x_i y_i - \sum_i x_i \sum_j x_j}{n \sum_i x_i^2 - \left(\sum_i y_i \right)^2} \qquad (39)$$

Computing was done using a Hewlett-Packard model 9100A programmable calculator. Computation of $\ln PT^{\frac{1}{2}}$ and $1/T$ was performed and equation (39) was applied to the data.

Because E_o and ω_g change slowly with temperature, data from narrow temperature intervals may be separately fit to equation (30). Parameters a and b may then be calculated for each temperature interval. The values of E_o and ω_g calculated then are referred to the temperature corresponding to the center of each interval.

In order to permit comparisons of the variations of E_o and ω_g for different gases, the temperature intervals chosen correspond to the same reduced temperature intervals for each gas. The temperature intervals used for this analysis are shown in Table 6. Reduced temperatures were calculated using parameters presented in Table 3.

TABLE 6

Temperature intervals used for analysis of vapor pressure equations.

Reduced temperatures (nondimensional)	Actual temperatures (K)		
	Ar	Kr	Xe
0.70 - 0.65	84.5 - 78.0	115 - 107	162 - 150
0.65 - 0.60	78.0 - 72.0	107 - 98.4	150 - 139
0.60 - 0.55	72.0 - 66.0	98.4 - 90.2	139 - 127
0.55 - 0.45	66.0 - 54.0	90.2 - 73.8	127 - 104
0.45 - 0.35	54.0 - 40.0	73.8 - 54.7	104 - 76.2

Columns 3 and 4 of Table 7 show values of the parameters a and b of equation (30). These parameters were calculated using the temperature intervals shown in Table 6. The values of a and b are found for pressures expressed in dynes/cm^2 in order to simplify calculation of E_o and ω_g in proper units.

TABLE 7

Values of the parameters a and b of equation (30) found from vapor pressure data.

Gas	Temperature Range (K)	-a(K)	b
Ar	84.5 - 78.0	988.74	27.4565
Ar	78.0 - 72.0	999.32	27.5921
Ar	72.0 - 66.0	995.01	27.5327
Ar	66.0 - 54.0	993.95	27.5150
Ar	54.0 - 40.0	1061.28	28.6928
Kr	115 - 107	1387.78	27.8683
Kr	107 - 98.4	1386.79	27.8608
Kr	98.4 - 90.2	1393.48	27.9299
Kr	90.2 - 73.8	1368.86	27.6426

(Table 7 continued)

Gas	Temperature Range (K)	-a(K)	b
Kr	73.8 - 54.7	1441.08	28.5093
Xe	162 - 150	1933.79	28.1399
Xe	150 - 139	1929.86	28.1137
Xe	139 - 127	1931.63	28.1250
Xe	127 - 104	1896.91	27.8466
Xe	104 - 76.2	2028.45	29.2002

Values of E_o and ω_g corresponding to these values of a and b are shown in the third and fourth columns of Table 8. These values of E_o and ω_g are referred to the temperatures in the second column.

TABLE 8

Values of E_o and ω_g calculated from the parameters of Table 7.

Gas	Temperature (K)	$-E_o$(cal/mole)	$\omega_g(10^{12}\text{sec}^{-1})$
Ar	81.2	1964	6.60
Ar	75.0	1985	6.91
Ar	69.0	1976	6.77
Ar	60.0	1974	6.73
Ar	47.0	2108	9.97
Kr	111	2756	5.23
Kr	103	2754	5.22
Kr	94.3	2768	5.34
Kr	82.0	2719	4.85
Kr	63.2	2862	6.48

(Table 8 continued)

Gas	Temperature (K)	$-E_o$(cal/mole)	$\omega_g(10^{12}sec^{-1})$
Xe	156	3841	4.57
Xe	145	3833	4.53
Xe	133	3837	4.55
Xe	115	3768	4.15
Xe	90.1	4029	6.51

A similar analysis was performed using equation (36). This equation is corrected to account for vacancy concentrations. The values of E_o and ω_g may be calculated from the parameters a and b of equation (36). These values will reflect the effect of vacancy formation and will differ slightly from those presented in Table 8.

Estimates of the effect of vacancy formation on specific heat measurements have yielded values for g_s, the Gibbs function for vacancy formation, for Ar and Kr.[41] These values may be expressed as:

for Ar, $\exp[-g_s/kT] = 30 \exp[-644.2/T(K)]$ and

for Kr, $\exp[-g_s/kT] = 30 \exp[-890.8/T(K)]$.

No vacancy concentration measurements were available for Xe so the value of g_s was estimated using the law of corresponding states. Using the definition, $g = u-Ts + Pv$, we have $\exp(-g_s/kT) = \exp[-(u-Ts+Pv)/kT]$.

This may be rewritten as $\exp(-g_s/kT) = (\exp s/k) \exp[(-u-Pv)/kT]$. The parameter s/k in the

first term is dimensionless so the reduced value is the same for Ar, Kr, and Xe. However, u + Pv has units of energy so that the appropriate reduced variable is $u + Pv/\epsilon$.

The reduced value of g_s for Xe was assumed to be equal to the average of the reduced values of g_s for Ar and Kr. Using the values of ϵ found in Table 3, the value of g_s for Xe was found to be

$$\exp(-g_s/kT) = 30 \exp\left[-1248/T(K)\right] .$$

Using the values reported above for $\exp(-g_s/kT)$, the experimental data for Ar, Kr, and Xe were fit to equation (36) and were plotted in Figures 9,10, and 11, respectively. Data were also fit to equation (36) by the method of least squares. Data from the temperature intervals shown in Table 6 were used for the fit. The values of a and b for each temperature interval are presented in Table 9. Values of a and b are again found for pressures expressed in dynes/cm^2 in order to simplify calculation of E_o and ω_g. Values of E_o and ω_g corresponding to these values of a and b are presented in Table 10.

TABLE 9

Values of the parameters a and b of equation (36) found from vapor pressure data.

Gas	Temperature Range (K)	-a(K)	b
Ar	84.5 - 78.0	995.89	27.5553
Ar	78.0 - 72.0	1004.12	27.6609
Ar	72.0 - 66.0	996.42	27.5557
Ar	66.0 - 54.0	994.62	27.5269
Ar	54.0 - 40.0	1061.30	28.6932
Kr	115 - 107	1396.12	27.9533
Kr	107 - 98.4	1390.84	27.9052
Kr	98.4 - 90.2	1395.47	27.9533
Kr	90.2 - 73.8	1378.55	27.7718
Kr	73.8 - 54.7	1439.73	27.7718
Xe	162 - 150	1945.65	28.2259
Xe	150 - 139	1932.43	28.1377
Xe	139 - 127	1934.22	28.1469
Xe	127 - 104	1855.76	27.5149
Xe	104 - 76.2	2007.64	28.9352

TABLE 10

Values of E_o and ω_g calculated from the parameters of Table 9.

Gas	Temperature (K)	$-E_o$(cal/mole)	$\omega_g(10^{12}sec^{-1})$
Ar	81.2	1978	6.82
Ar	75.0	1994	7.07
Ar	69.0	1979	6.82
Ar	60.0	1976	6.76
Ar	47.0	2108	9.97
Kr	111	2773	5.38
Kr	103	2762	5.29
Kr	94.3	2772	5.38
Kr	82.0	2738	5.06
Kr	63.2	2860	6.42
Xe	156	3864	4.71
Xe	145	3838	4.57
Xe	133	3842	4.58
Xe	115	3686	3.71
Xe	90.1	3988	5.96

Heat of Sublimation

The data were also analyzed using equation (23) to calculate values for the heat of sublimation, L. The data are plotted in the form ln P(Torr) versus $1/T$ in Figures 12, 13, and 14. The techniques described in the previous Section were used to fit the data to equation (23) by the method of least squares. As in the previous Section, the parameter a was expected to vary slowly with temperature. Because of the expected variation, data from the temperature intervals of Table 6 were used for the fit. As before, the data from each interval were fit to equation (23) separately. Thus, the values of the parameter a are referred again to the temperatures at the centers of the intervals.

The heat of sublimation, L, is related to the parameter a of equation (23) by:

$$a = \frac{L}{R\,(1 - v_s/v_g + BP/RT)} \quad . \quad (40)$$

The parameter a was determined from the least square fit described earlier. The specific volumes of the solids, v_s, were obtained from density curves.[2] Values of the second virial coefficient, B, were obtained from an extrapolation of reduced curves.[42]

Values found for the parameters a and b of equation (23) are presented in Table 11. Calculated values of heats of sublimation are presented in Table 12.

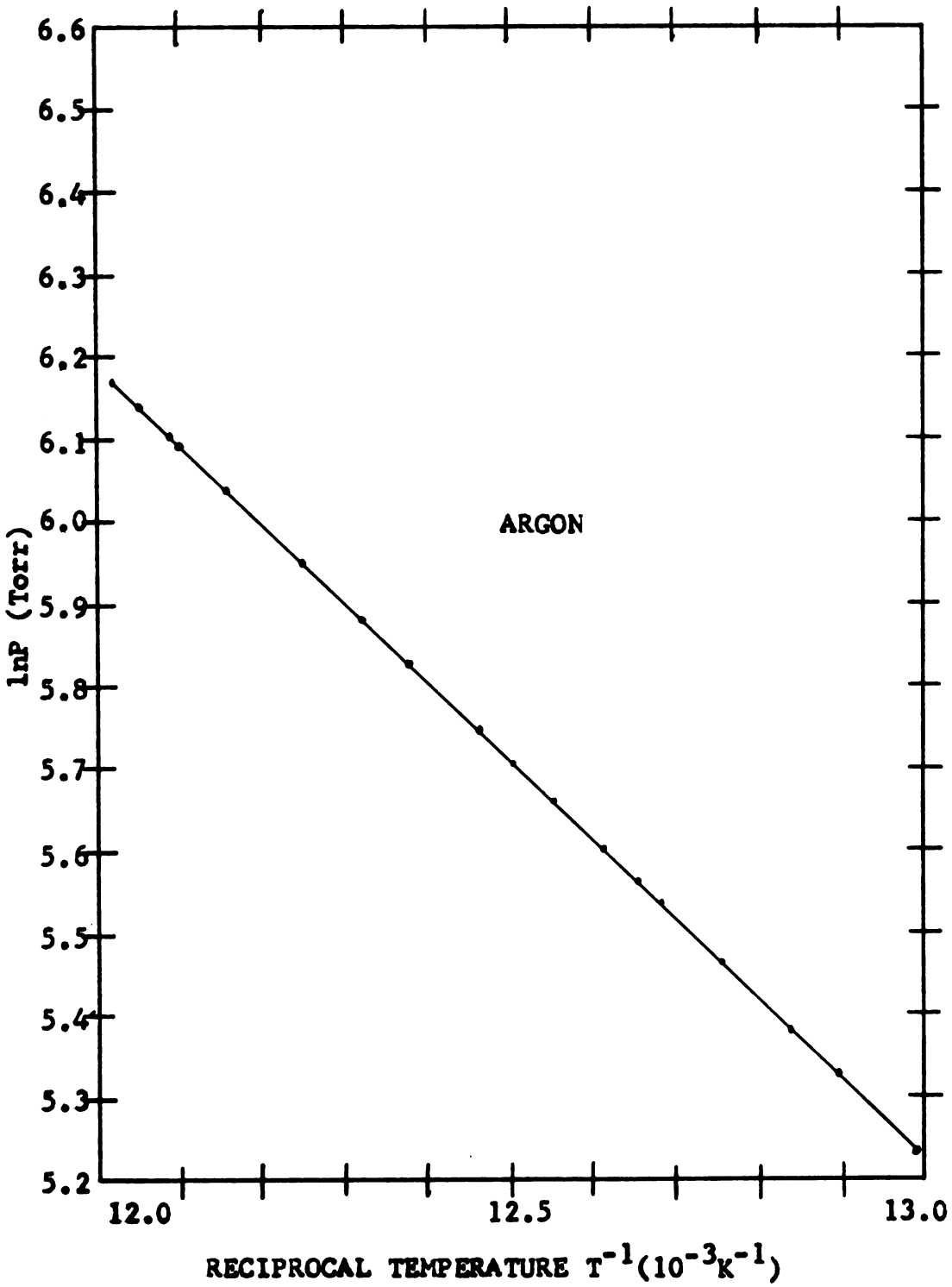

Figure 12: Typical plot of lnP versus 1/T for Ar.

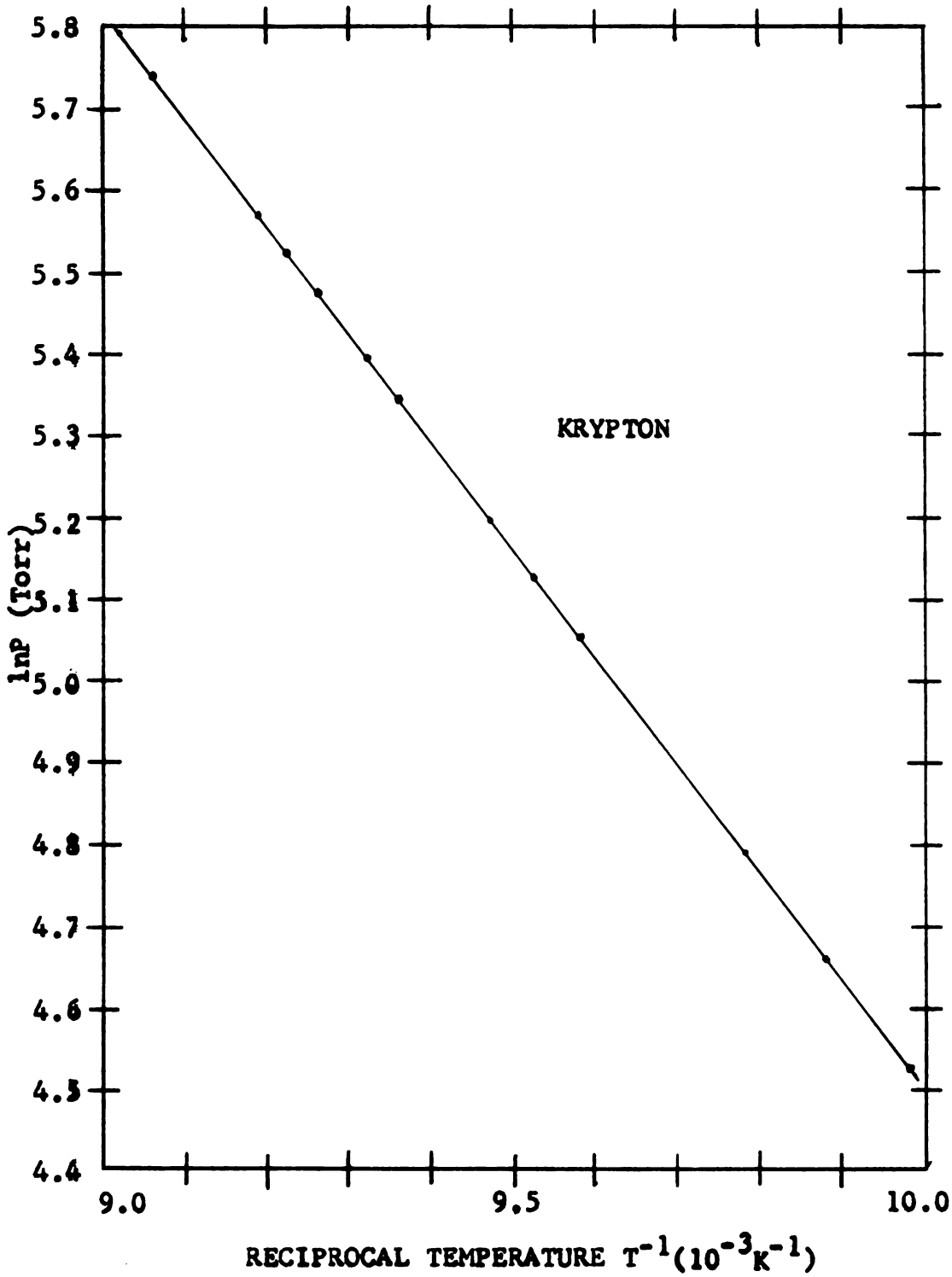

Figure 13: Typical plot of lnP versus 1/T for Kr.

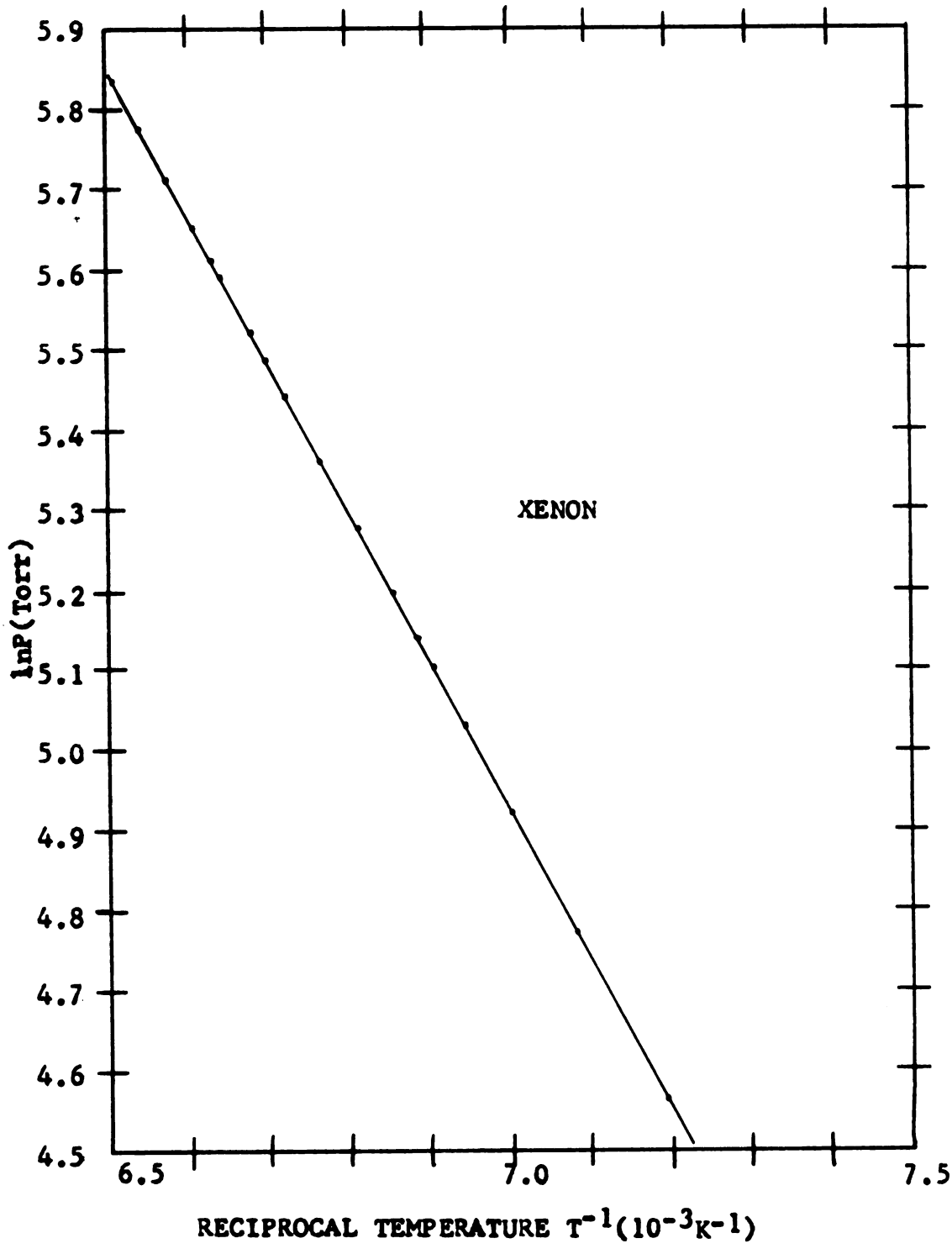

Figure 14: Typical plot of lnP versus 1/T for Xe.

TABLE 11

Values of the parameters a and b of equation (23) found from vapor pressure data.

Gas	Temperature Range (K)	-a(K)	b
Ar	84.5 - 78.0	946.35	17.5408
Ar	78.0 - 72.0	962.22	17.7428
Ar	72.0 - 66.0	960.59	17.7214
Ar	66.0 - 54.0	963.39	17.7623
Ar	54.0 - 40.0	1038.03	19.0767
Kr	115 - 107	1332.30	17.8184
Kr	107 - 98.4	1334.63	17.8413
Kr	98.4 - 90.2	1346.76	17.9656
Kr	90.2 - 73.8	1330.73	17.7765
Kr	73.8 - 54.7	1399.08	18.5731
Xe	162 - 150	1856.41	17.9236
Xe	150 - 139	1857.02	17.9276
Xe	139 - 127	1860.70	17.9513
Xe	127 - 104	1836.37	17.7526
Xe	104 - 76.2	1960.37	18.9607

TABLE 12

Values of heat of sublimation, L, calculated from the parameters of Table 11.

Gas	Temperature (K)	L (cal/mole)
Ar	81.2	1852
Ar	75.0	1900
Ar	69.0	1904
Ar	60.0	1914
Ar	47.0	2062
Kr	111	2612
Kr	103	2636
Kr	94.3	2670
Kr	82.0	2644
Kr	63.2	2780
Xe	156	3480
Xe	145	3596
Xe	133	3661
Xe	115	3632
Xe	90.1	3895

Lattice Vibrational Energy

The lattice vibrational energy, E_{vib}, may now be calculated using the thermodynamic relation,

$$E_{vib} = -E_o - L + P(v_g - v_s) \quad . \quad (41)$$

Physically, this equation is similar to the equation $E_z(0K) = -E_o(0K) - L(0K)$. This latter equation defines the zero-point vibrational energy at 0 K. Equation (41) applies for temperatures above 0 K; thus, the work done by expanding gases must be subtracted from the heat of sublimation. This adds the term $P(v_g - v_s)$ which represents the amount of work done by expanding gases removed from the solid.

The specific volumes, v_s and v_g, of equation (41) are the same as those used to calculate the heats of sublimation.[2] The calculated values of E_{vib} are presented in Table 13.

TABLE 13

Values of vibrational energy, E_{vib}, calculated using equation (41).

Gas	Temperature (K)	E_{vib} (cal/mole)
Ar	81.2	285
Ar	75.0	243
Ar	69.0	213
Ar	60.0	181
Ar	47.0	139
Kr	111	381
Kr	103	331
Kr	94.3	288
Kr	82.0	258
Kr	63.2	205
Xe	156	693
Xe	145	529
Xe	133	445
Xe	115	281
Xe	90.1	272

V. GENERAL CONCLUSION

As can be seen from Figure 5, Figure 6, and Figure 7, the sublimation pressures of solid Ar, Kr, and Xe have been measured over several orders of magnitude. However, for each gas the pressure curves began to level off at low pressures.

The cause of this deviation was the presence of non-condensable impurities such as He in our gas samples. As the sample temperature was lowered, most of the primary gas component was condensed. The concentration of non-condensable impurities then became large in the vapor phase. The vapor pressure curve then began to level off because lowering the sample temperature further had little effect on the vapor phase.

These curves were reproducible for different gas samples and different runs. This indicates that the impurities were present in our gas samples and not evolved from the walls of the gas handling system. If the data had not been repeatable or had changed with the length of time the samples had been contained in the system, this would have indicated that outgassing of our system was contaminating the sample.

Assuming the impurities present were non-condensable gases such as He, it was possible to estimate the concentration of the impurities present in the gas samples. This was done by assuming that the original gas pressure before the sample was condensed was the pressure due to the primary gas component plus the partial pressure of the impurities. The lowest vapor pressure measured then was equal to the partial pressure of the non-condensable impurity gases.

Assuming that the ratio of the partial pressure of impurities to the total gas pressure equals the impurity concentration, the impurity concentration may be calculated. The estimated impurity concentrations found from this analysis are: 0.2 ppm for Ar, 13 ppm for Kr, and 10 ppm for Xe. These values may be compared with the impurity levels reported in Table 4.

The estimated values are probably accurate for Ar but may not be so reliable for Kr and Xe. For these latter two gases, the partial pressure at the lowest temperatures measured of condensed impurities such as N_2 and O_2 at the lowest temperatures measured, may be higher because the sample temperature is higher. A further source of inaccuracy at low temperatures is the correction for thermal transpiration. Even though the gas inlet tube used was of relatively large diameter (¼in. i.d.) this correction became large at low temperatures. The anomalously low values of static lattice

energies and heats of sublimation for reduced temperatures, $T^* \approx 0.5$, indicate a large overcorrection for thermal transpiration.

Thus it is expected that actual vapor pressures below 0.1 Torr should be somewhat higher than observed. This effect is masked at still lower temperatures at which the measured pressure is increased due to impurities. For better low temperature measurements, an improved correction for thermal transpiration and improved techniques for gas purification are required.

At high temperatures our data may be compared with that of previous workers. Most previously available data is reported in terms of the parameters a and b in equation (23). For comparison with our results some of the values for a and b found by other workers follow. For the temperature interval 83.6 - 66.1K Flubacher *et al.*[43] found a = -953.897K, b = 17.62836 for Ar. For the temperature interval 115.8 - 83.3K, Beaumont *et al.*[41] found a = -1127.58K, b = 16.04625 for Kr. For the temperature interval 161 - 110K, Freeman and Halsey found a = -1840.0 and b = 16.972 for Xe. Our parameters calculated for Kr differ significantly from those found by Beaumont *et al.* but are closer to the parameters a = -1346 and b = 17.833 found earlier by Freeman and Halsey[44] for the temperature interval 115 - 80 K.

LIST OF REFERENCES

LIST OF REFERENCES

1. E.R. Dobbs and G.O. Jones, Repts. Progr. Phys 20, 516 (1957).

2. G.L. Pollack, Rev. Mod. Phys. 36, 748 (1964).

3. G.K. Horton, Am. J. Phys. 36, 93 (1968).

4. M.L. Klein, J. Chem. Phys. 41, 749 (1964).

5. M.L. Klein and J.A. Reissland, J. Chem. Phys. 41, 2773 (1964).

6. L. Jansen, Phil. Mag. 8, 1305 (1965).

7. L.S. Salter, Trans. Faraday Soc. 59, 657 (1963).

8. D.L. Losee and R.O. Simmons, Phys. Rev. Letters 18, 451 (1967).

9. R. Becker, Theorie der Wärme (Springer-Verlag, Berlin, 1953) p. 38.

10. L.I. Schiff, Quantum Mechanics (McGraw-Hill, New York, 1968) p. 261.

11. E.A. Mason and W.E. Rice, J. Chem. Phys. 22, 843 (1954).

12. R.M.J. Cotterill and M. Doyama, Phys. Letters 25A, 35 (1967).

13. R.J. Munn and F.J. Smith, J. Chem. Phys. 43, 3998 (1965).

14. G.K. Horton and J.W. Leech, Proc. Phys. Soc. (London) 82, 816 (1963).

15. E.A. Guggenheim and M.L. McGlashan, Proc. Phys. Soc. (London) A255, 456 (1960).

16. E.A. Guggenheim, J. Chem. Phys. 13, 253 (1945).

17. J.E. De Boer, Physica 14, 139 (1948).

18. J.E. De Boer and B.S. Blaisse, Physica 14, 149 (1948).

19. T.H.K. Barron and C. Domb, Proc. Roy. Soc. (London) A227, 447 (1955).

20. L. Jansen and R.T. McGinnis, Phys. Rev. 104, 961 (1956).

21. C.S. Barrett and L. Meyer, J. Chem. Phys. 42, 107 (1965).

22. B.J. Alder and R.H. Paulson, J. Chem. Phys. 43, 4172 (1965).

23. L. Jansen, Phys. Letters 4, 91 (1963).

24. F. Sears, Thermodynamics (Addison-Wesley, Reading), 161 (1959).

25. Y. Larher, J. Chim. Phys. 65, 114 (1968).

26. L.H. Bolz, H.P. Broida, and H.S. Peiser, Acta Cryst. 15, 810 (1962).

27. E.D. Hondras and A.J.W. Moore, Acta Met. 8, 647 (1960).

28. G.K. White, Experimental Techniques in Low Temperature Physics, (Oxford Press, London) 104, (1961).

29. F.B. Rolfson in Temperature its Measurement and Control in Science and Industry.(Rheinhold Publishing Co., New York) Vol. 3, ed. AI. Dahl, part 2, 787 (1962).

30. Comité International des Poids et Mesures, Metrologia 5, 35 (1969).

31. H.L. Daneman and G.C. Mergner, Inst. Tech. 14, 51 (1967).

32. J. Kistemaker, Physica 11, 277 (1945).

33. AIP Handbook (McGraw-Hill Book Co., New York) editor Dwight E. Gray, 2-140 (1957).

34. A.E. de Vries and P.K. Rol, Vacuum 15, 135 (1965).

35. Handbook of Chemistry and Physics (Chemical Rubber Publishing Co., Cleveland, Ohio) edited by Charles D. Hodgeman, 2368 (1961).

36. S. Dushman, Scientific Foundations of Vacuum Technique, John Wiley and Sons, Inc., New York), 59 (1962).

37. T. Takeishi and Y. Sensui, Trans. Faraday Soc. 59, 2503 (1963).

38. G.L. Pollack, Phys. Rev. A1 (to be published).

39. G. Boato and G. Casanova, Physica 27, 571 (1961).

40. C. Mack, Essentials of Statistics for Scientists and Technologists, (Plenum Publishing Co., New York), 107 (1966).

41. R.H. Beaumont, H. Chihara, and J.A. Morrison, Proc. Phys. Soc. (London) 78, 1462 (1961).

42. L. Bewilogua and C. Gladun, Contemp. Phys. 9, 277 (1968).

43. P. Flubacher, A.J. Leadbetter, and J.A. Morrison, Proc. Phys. Soc. (London) 78, 1449 (1961).

44. M.P. Freeman and G. D. Halsey, Jr., J. Phys. Chem. 60, 1119 (1956).

APPENDIX

APPENDIX

TABLE A1

Measured pressure and temperature points for Ar.

Ar		Ar	
Pressure (Torr)	Temperature (K)	Pressure (Torr)	Temperature (K)
561.099	84.495	53.339	69.886
538.557	84.128	53.106	69.867
513.970	83.730	49.988	69.560
492.247	83.412	46.716	69.219
464.519	82.994	41.593	68.643
448.290	82.742	37.246	68.106
443.067	82.661	36.375	67.992
420.063	82.266	34.477	67.735
385.901	81.666	32.091	67.397
358.409	81.155	28.104	66.777
340.153	80.797	26.967	66.586
313.180	80.238	24.661	66.178
299.849	79.947	22.703	65.802
284.865	79.647	19.304	65.080
271.425	79.287	17.436	64.637
261.737	79.038	16.172	64.312
254.242	78.858	14.199	63.754
236.758	78.399	13.547	63.556
218.673	77.892	10.636	62.552
204.450	77.463	8.132	61.521
189.298	76.984	4.703	59.443
173.501	76.444	3.983	58.808
167.508	76.226	3.243	58.095
159.117	75.916	2.212	56.608
145.576	75.383	0.601	52.488
128.462	74.613	0.204	50.018
119.122	74.286	0.0675	47.845
114.188	74.000	0.0660	47.739
98.050	73.138	0.0262	45.929
90.947	72.719	0.0218	45.492
79.972	72.013	0.0158	44.807
73.900	71.589	0.0108	44.015
68.564	71.191	7.5×10^{-3}	43.160
62.115	70.673	6.0×18^{-3}	42.769
57.647	70.286	3.8×10^{-3}	41.871

(Table A1 continued)

Ar Pressure (Torr)	Ar Temperature (K)	Ar Pressure (Torr)	Ar Temperature (K)
8.2×10^{-4}	38.707	5.0×10^{-6}	29.099
2.2×10^{-4}	36.803	3.5×10^{-6}	27.601
7.0×10^{-5}	34.977	3.4×10^{-6}	27.525
3.4×10^{-5}	33.930	2.7×10^{-6}	26.065
1.5×10^{-5}	32.146	2.3×10^{-6}	25.506
8.7×10^{-6}	30.400		

TABLE A2

Measured pressure and temperature points for Kr.

Kr		Kr	
Pressure (Torr)	Temperature (K)	Pressure (Torr)	Temperature (K)
505.261	114.914	92.135	100.213
502.293	114.855	82.361	99.378
482.453	114.457	73.122	98.506
460.901	114.010	62.813	97.418
441.980	113.608	56.989	96.734
421.227	113.141	51.082	95.974
417.699	113.072	43.539	94.889
400.137	112.649	39.466	94.238
393.148	112.494	21.663	90.450
380.794	112.179	20.965	90.250
370.278	111.939	20.202	90.029
359.921	111.650	19.003	89.660
351.269	111.433	18.953	89.644
341.909	111.169	17.324	89.114
327.079	110.772	14.773	88.189
318.285	110.512	13.995	87.877
310.807	110.305	12.781	87.366
300.348	109.982	12.709	87.328
287.134	109.600	11.733	86.882
283.954	109.476	10.923	86.468
263.805	108.828	10.044	86.027
261.753	108.746	8.820	85.316
249.681	108.341	7.754	84.635
241.268	108.029	7.065	84.138
238.618	107.926	6.733	83.879
209.386	107.799	5.893	83.215
222.243	107.317	5.387	82.761
221.013	107.279	4.549	81.896
209.386	106.799	3.604	80.746
193.818	106.138	3.181	80.156
181.424	105.588	2.525	79.054
175.569	105.304	2.110	78.199
168.667	104.978	1.962	77.853
160.055	104.504	1.554	76.773
156.598	104.370	1.133	75.278
147.423	103.886	0.841	74.027
128.521	102.776	0.523	72.279
123.549	102.463	0.389	71.057
119.813	102.226	0.295	70.342
113.961	101.834	0.186	68.663
105.260	101.224	0.140	68.070
98.954	100.749	0.131	67.589

(Table A2 continued)

Kr		Kr	
Pressure (Torr)	Temperature (K)	Pressure (Torr)	Temperature (K)
0.092	66.822	7.5×10^{-3}	59.727
0.0879	66.590	4.6×10^{-3}	58.304
0.0619	65.675	3.5×10^{-3}	57.565
0.0608	65.620	2.1×10^{-3}	56.297
0.0467	64.909	1.7×10^{-3}	55.415
0.0337	64.084	1.0×10^{-3}	54.380
0.0231	63.138	8.6×10^{-4}	53.467
0.0172	62.152	5.2×10^{-4}	51.961
0.0136	61.244	3.0×10^{-4}	49.259
0.0119	61.128	2.1×10^{-4}	46.017
8.0×10	60.122	2.1×10^{-4}	45.130

TABLE A3

Measured pressure and temperature points for Xe.

Xe		Xe	
Pressure (Torr)	Temperature (K)	Pressure (Torr)	Temperature (K)
505.969	158.710	81.521	137.310
496.632	158.458	74.512	136.409
486.381	158.170	74.491	136.400
465.899	157.588	67.318	135.403
444.649	156.972	65.980	135.198
424.359	156.354	64.131	134.931
403.954	155.706	58.299	134.006
383.428	155.028	57.887	133.928
373.930	154.709	52.315	132.972
363.577	154.342	50.895	132.699
355.436	154.058	47.631	132.088
342.665	153.582	44.742	131.498
335.974	153.341	42.894	131.117
322.624	152.820	39.719	130.405
316.179	152.579	38.325	130.088
302.091	151.999	35.224	129.326
295.350	151.727	34.664	129.176
284.928	151.282	31.178	128.240
281.254	151.114	30.294	127.978
273.829	150.798	28.910	127.577
270.013	150.607	28.844	127.543
268.649	150.561	26.533	126.822
252.950	149.831	26.367	126.764
250.344	149.692	25.702	126.538
249.147	149.645	24.894	126.279
241.695	149.296	23.177	125.686
235.097	148.949	22.829	125.544
231.717	148.781	20.236	124.530
230.188	148.684	20.168	124.520
213.153	147.800	18.011	123.585
205.518	147.350	17.567	123.358
196.376	146.840	15.988	122.613
187.374	146.271	15.575	122.375
181.283	145.921	14.222	121.671
170.785	145.211	13.940	121.485
166.702	144.965	12.475	120.640
154.186	144.088	12.227	120.448
153.757	144.058	10.963	119.599
139.989	142.018	9.661	118.619
138.631	142.831	3.594	111.004
128.865	142.115	2.859	109.519
118.179	141.183	2.323	108.183
100.106	139.419	1.809	106.962
96.094	138.992	1.383	105.018
90.905	138.418	1.034	103.316
84.552	137.680	0.767	101.672

(Table A3 continued)

Xe		Xe	
Pressure (Torr)	Temperature (K)	Pressure (Torr)	Temperature (K)
0.367	97.826	7.2×10^{-3}	81.923
0.246	95.935	5.6×10^{-3}	81.528
0.162	94.136	4.8×10^{-3}	80.982
0.132	93.106	4.3×10^{-3}	80.806
0.106	92.117	3.4×10^{-3}	79.587
0.0843	91.759	2.9×10^{-3}	78.865
0.0522	89.851	2.3×10^{-3}	78.082
0.0321	88.013	1.6×10^{-3}	76.474
0.0205	86.253	1.4×10^{-3}	76.034
0.0179	85.963	8.1×10^{-4}	74.054
0.0136	84.830	6.0×10^{-4}	72.522
0.0108	83.646	4.7×10^{-4}	71.372
9.0×10^{-3}	83.02	3.8×10^{-4}	70.075